Nuclear Inst. and Methods in Physics Research, A 1049 (2023) 168040

Contents lists available at ScienceDirect

Nuclear Inst. and Methods in Physics Research, A

journal homepage: www.elsevier.com/locate/nima

Full Length Article

Conceptual design of the AGATA 2π array at LNL

J.J. Valiente-Dobón [a,*], R. Menegazzo [b], A. Goasduff [a], D. Agguiaro [b], P. Aguilera [b], F. Angelini [a,c], M. Balogh [a], D. Bazzacco [b], J. Benito [b,c], G. Benzoni [d], N. Bez [b], M. Bolognesi [c], S. Bottoni [e], D. Brugnara [a], S. Carollo [b,c], P. Cocconi [a], A. Cogo [a], J. Collado [a,f], F.C.L. Crespi [e], A. Ertoprak [a], R. Escudeiro [b,c], F. Galtarossa [a,c], E.R. Gamba [e], A. Gambalonga [a], B. Góngora Servín [a,g], A. Gottardo [a], A. Gozzelino [a], M. Gulmini [a], Z. Huang [b,c], T. Marchi [a], D. Mengoni [b,c], P. Modanese [a], D.R. Napoli [a], J. Pellumaj [a,g], R.M. Pérez-Vidal [a,h], S. Pigliapoco [b,c], E. Pilotto [a,c], L. Ramina [b], M. Rampazzo [b], W. Raniero [a], M. Rebeschini [b], K. Rezynkina [b], D. Rosso [a], M. Scarcioffolo [c], D. Scarpa [a], M. Sedlák [a], R. Smith [i], N. Toniolo [a], F. Veronese [b], V. Volpe [a], L. Zago [a,c], I. Zanon [a], G. Zhang [b,c], R. Abels [j], M.L. Allegrini [a], C. Aufranc [k], G. Baulieu [k], C. Belkhiria [l], M. Benettoni [b], D. Benini [a], M. Bentley [u], M. Biasotto [a], M. Blaizot [l], J. Blasco Miquel [h], C. Boiano [d], A. Boston [m], H. Boston [m], A. Boujrad [l], P. Bourgault [l], A. Bracco [d,e], S. Brambilla [d], I. Burrows [i], F. Camera [d,e], S. Capra [d,e], A. Capsoni [d], R. Cash [i], J.V. Civera [h], E. Clément [l], S. Coelli [d], M. Cordwell [i], L. Corradi [a], S. Coudert [l], G. De Angelis [a], L. De Ruvo [a], G. Debras [n], M. Del Fabbro [b,c], J. Diklić [o], N. Dosme [p], G. Duchene [q], B. Duclos [l], J. Dudouet [k], J. Eberth [j], S. Elloumi [p], C. Everett [m], S. Fantinel [a], M. Fillinger [q], E. Fioretto [a], C. Fransen [j], A. Gadea [h], L. Gibelin [p], V. González [f], J. Goupil [l], C. Görgen [j], A. Grant [i], K. Green [m], J. Ha [b,c], T. Hartnett [i], K. Henseler [j], H. Hess [j], R. Hirsch [j], C. Houarner [l], J. Jacob [p], T. Joannem [n], D.S. Judson [m], N. Karkour [p], M. Karolak [n], M. Kebbiri [n], J. Kieffer [n], M. Labiche [i], X. Lafay [p], P. Le Jeannic [p], A. Lefevre [l], E. Legay [p], F. Legruel [l], S. Lenzi [c,b], S. Leoni [e,d], D. Linget [p], M. Liptrot [i], A. López-Martens [p], A. Lotodé [n], L. Manara [d], L. Ménager [l], T. Mijatović [o], B. Million [d], A. Minarello [a], G. Montagnoli [c,b], P. Morrall [i], I. Mullacrane [i], J. Nyberg [t], G. Philippon [p], M. Polettini [e], F. Popieul [n], A. Pullia [e,d], F. Recchia [b,c], P. Reiter [j], G. Richardt [j], M. Rocchini [r], A. Roger [n], F. Saillant [l], E. Sanchis [f], Md.S.R. Laskar [d], G. Secci [e,d], M.-H. Sigward [q], J. Simpson [i], N. Solenne [n], F. Spee [j], A.M. Stefanini [a], O. Stézowski [k], S. Szilner [o], N. Templeton [i], Ch. Theisen [n], S. Thiel [j], F. Tomasi [d], S. Tzvetkov [n], D. Vigano [d], E. Viscione [d], O. Wieland [d], K. Wimmer [s], G. Wittwer [l], M. Zielińska [n]

[a] *Istituto Nazionale di Fisica Nucleare (INFN), Laboratori Nazionali di Legnaro, Legnaro, Italy*
[b] *Istituto Nazionale di Fisica Nucleare (INFN), Sezione di Padova, Padova, Italy*
[c] *Dipartimento di Fisica, Università di Padova, Padova, Italy*
[d] *Istituto Nazionale di Fisica Nucleare (INFN), Sezione di Milano, Milano, Italy*
[e] *Dipartimento di Fisica, Università degli Studi di Milano, Milano, Italy*
[f] *Departamento de Ingeniería Electrónica, Universitat de Valencia, Burjassot, Valencia, Spain*
[g] *Dipartimento di Fisica e Scienze della Terra, Università di Ferrara, Ferrara, Italy*
[h] *IFIC, CSIC - Universitat de València, Spain*
[i] *Science and Technology Facilities Council (STFC), Daresbury Laboratory, Keckwick Lane, Warrington, UK*
[j] *Institut für Kernphysik, Universität zu Köln, Köln, Germany*
[k] *Université Lyon, Université Claude Bernard Lyon , CNRS/IN2P3, IP2I Lyon, France*
[l] *Grand Accélérateur National d'Ions Lourds (GANIL), CEA/DRF-CNRS/IN2P3, Caen, France*
[m] *Oliver Lodge Laboratory, University of Liverpool, Liverpool, UK*
[n] *IRFU, CEA, Université Paris-Saclay, Gif-sur-Yvette, France*
[o] *Ruđer Bošković Institute, Zagreb, Croatia*

* Corresponding author.
E-mail address: valiente@lnl.infn.it (J.J. Valiente-Dobón).

https://doi.org/10.1016/j.nima.2023.168040
Received 22 November 2022; Received in revised form 18 December 2022; Accepted 14 January 2023
Available online xxxx
0168-9002/© 2023 Elsevier B.V. All rights reserved.

[p] IJClab, Université Paris Saclay, CNRS, Orsay, France
[q] IPHC, UMR 7178, CNRS/IN2P3, Université de Strasbourg, Strasbourg, France
[r] Department of Physics, University of Guelph, Guelph, Canada
[s] GSI Helmholtzzentrum für Schwerionenforschung, Darmstadt, Germany
[t] Department of Physics and Astronomy, Uppsala University, Uppsala, Sweden
[u] Department of Physics, University of York, York, UK

ARTICLE INFO

Keywords:
AGATA spectrometer
LNL facility
γ-ray tracking
Pulse shape analysis
PRISMA spectrometer
EUCLIDES detector
DANTE detector
TRACE detector
Plunger device

ABSTRACT

The Advanced GAmma Tracking Array (AGATA) has been installed at Laboratori Nazionali di Legnaro (LNL), Italy. In this installation, AGATA will consist, at the beginning, of 13 AGATA triple clusters (ATCs) with an angular coverage of 1π, and progressively the number of ATCs will increase up to a 2π angular coverage. This setup will exploit both stable and radioactive ion beams delivered by the Tandem–PIAVE-ALPI accelerator complex and the SPES facility. The new implementation of AGATA at LNL will be used in two different configurations, firstly one coupled to the PRISMA large-acceptance magnetic spectrometer and lately a second one at Zero Degrees, along the beam line. These two configurations will allow us to cover a broad physics program, using different reaction mechanisms, such as Coulomb excitation, fusion-evaporation, transfer and fission at energies close to the Coulomb barrier. These setups have been designed to be coupled with a large variety of complementary detectors such as charged particle detectors, neutron detectors, heavy-ion detectors, high-energy γ-ray arrays, cryogenic and gasjet targets and the plunger device for lifetime measurements. We present in this paper the conceptual design, characteristics and performance figures of this implementation of AGATA at LNL.

1. Introduction

The main objective of nuclear structure is the study of the nature and the phenomenology of nucleon–nucleon interaction in the nuclear medium and its emerging phenomena. High-resolution γ-ray spectroscopy plays a major role in this field, allowing for the measurement of physical observables related to the decay of the excited nuclear levels. From this precise measurement of the γ rays emitted from excited nuclear levels one obtains not only the excitation energy but also the reduced transition probabilities and their associated quantum numbers, by measuring: (i) the lifetime of excited states, from which one can deduce the reduced transition matrix elements, (ii) the γ-ray angular distributions, linked to the multipolarity of the transition and (iii) its polarization, which can provide information on the electric or magnetic character of the transition. Over five decades of developments in in-beam γ-ray spectroscopy, different experimental methods have been developed to measure all these quantities, significantly advancing our understanding of nuclear structure and the underlying nucleon–nucleon interaction. At present, state-of-the-art γ spectrometers for high-resolution γ spectroscopy are based on γ-ray tracking, such as the European project Advanced Gamma Tracking Array (AGATA) [1] and the USA project Gamma-Ray Energy In-beam Nuclear Array (GRETINA) [2]. Such a technology provides superior efficiency, position resolution and Doppler correction, improving the resolving power compared to conventional γ-ray spectrometers, thus boosting the study of rarer nuclear phenomena.

AGATA was first implemented at Laboratori Nazionali di Legnaro (LNL) in the so called demonstrator phase in 2009 [3], where it was coupled to the large acceptance magnetic spectrometer PRISMA [4–7] as well as other charged particle detectors. Then it moved to Helmholtzzentrum für Schwerionenforschung (GSI) to be positioned at the final focal position of the FRagment Separator (FRS) [8–10]. After GSI, AGATA in its 1π configuration was moved to the Grand Accélérateur National d'Ions Lourds (GANIL) [11]. The new implementation of AGATA at LNL in a 2π configuration represents the so called PHASE2 of AGATA, aiming to the completion of the 4π array. In this installation, AGATA will consist at the beginning of 13 AGATA triple clusters (ATCs) and the number of ATCs will increase with time up to 27 out of the 30 possible ATCs due to the mechanical constrains to get the beam line through. This setup will be employed with both stable beams from the TANDEM-ALPI-PIAVE accelerator complex and radioactive ion beams from SPES [12]. A rich physics program will be covered with AGATA and a pletora of complementary detectors such as the PRISMA spectrometer, particle detectors EUCLIDES [13,14], TRACE [15], SPIDER [16] and GRIT [17,18], the neutron detector NEDA [19], the γ-ray spectrometer PARIS [20], the plunger device [21], the heavy-ion detector DANTE [22] and the cryogenic and gas jet targets CTADIR [23] and SUGAR [24].

These setup, including the different complementary detectors, have been designed to study the structure of moderately neutron-rich nuclei populated by reactions such as multi-nucleon transfer, fusion–fission and transfer induced fission using Pb and U, neutron-deficient nuclei populated via fusion-evaporation reactions, Coulomb excitation and transfer reactions of stable and SPES ISOL beams. Previous campaigns at LNL and GANIL have produced rich physics results using similar setups [25]. The physics campaign at LNL will be further enriched by the usage of ^{238}U and ^{232}Th targets. The accelerator complex at LNL has been also upgraded to provide to the users ^{238}U beams.

In this manuscript, we will describe the conceptual design of the AGATA 2π array at LNL coupled to the various complementary detectors. Detailed simulations to investigate the performances of AGATA will also be discussed. This installation comprises a major upgrade of the AGATA infrastructures from the previous campaigns to accommodate a larger number of detectors towards the AGATA 2π configuration.

2. Description of the setup installation

The conceptual design of the AGATA 2π array at LNL coupled to the various complementary detectors has been conceived in order to optimize the geometry of the setup for the experimental activity foreseen at LNL. For example, AGATA in its first configuration, has been placed symmetrically along the optical axis of the PRISMA spectrometer at 180°. This is the optimal position to minimize the Doppler broadening. During the design it has been also taken into account that AGATA has been designed to work at any focal position (different target-to-detector distances) increasing its efficiency without significant looses in the resolution and peak-to-total performance. All the ancillary detectors have been also though in order to optimize the performance of AGATA coupled to the ancillary detectors. This setup is an upgrade of the previous implementations at LNL [3], GSI [8–10] and GANIL [11].

The AGATA 2π array has been installed at LNL. Two different configurations are foreseen, firstly one at the target position of the magnetic spectrometer PRISMA and a second one at Zero Degrees, where the beam line will pass along the symmetry axis of the AGATA spectrometer. These two setups will allow to pursue the rich physics program proposed by the community. The detector support system and

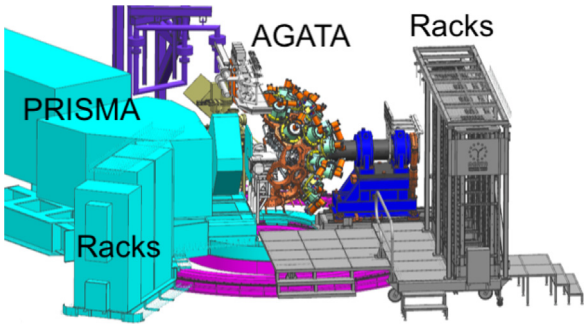

Fig. 1. General layout of AGATA 2π coupled to PRISMA installed at LNL (INFN). Racks that host the digitizers and the LVPS (gray), racks that host the liquid nitrogen autofill system, the electronics for the complementary detectors and the High Voltage System for the AGATA (cyan). PRISMA is also represented in cyan. See text for more details.

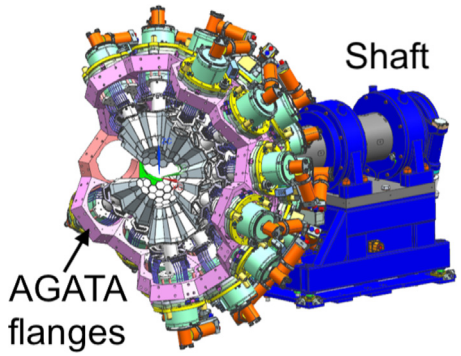

Fig. 2. The AGATA holding structure, together with thirty flanges in the honeycomb structure, built for the installation of AGATA at LNL. The shaft allows the rotation of AGATA ± 85° around its symmetry axis.

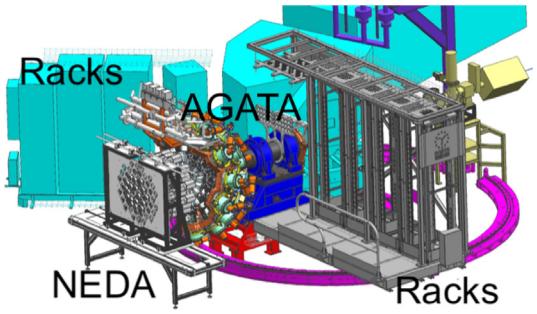

Fig. 3. General layout of AGATA 2π installed at LNL (INFN) for the Zero Degrees configuration with the neutron detector array NEDA [19]. Racks that host the digitizers and the LVPS (gray), racks that host the liquid nitrogen autofill system, the electronics for the complementary detectors and the High Voltage System for the AGATA (cyan).

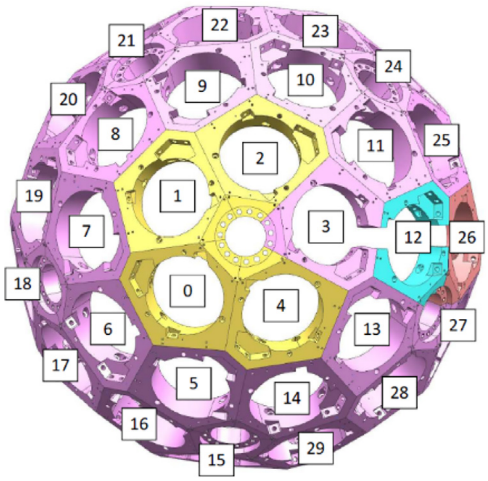

Fig. 4. The AGATA detector support at LNL with 30 flanges. The numbering of the honeycomb flanges follows the logic of the previous installations. The cut flanges 3, 12 and 26 are shown on the left in Fig. 2.

the front-end electronics are installed close to the array. In Fig. 1, where AGATA is shown coupled to PRISMA, the racks that host the digitizers and the Low Voltage Power Supply (LVPS) can be seen on the right. This platform presented large constraints during its design since the signal cables of the detectors to the digitizers have a limited length of 11 meters to keep the integrity of the signals. On the left of Fig. 1, instead, one can see the racks that host the liquid nitrogen autofill system, the electronics for the complementary detectors and the High Voltage System for the AGATA detectors. The electromagnetic compatibility between the different mechanical parts and the AGATA detector structure was carefully checked during the installation and various modifications were performed to comply with the specifications. Special care has been put in cable management, each ATC needs 29 cables that are collected in a bundle of about 70 mm in diameter. During the roto-translation of AGATA, the torsional efforts appear causing the bundles to roll up on themselves, in order to keep the integrity of the cables and avoid transmitting stress to the connectors, two cable bundles (one on the shaft and other on the racks) on the left in Fig. 1 were adopted along the path of the cables and protective PVC elements were inserted in these two points where the cables are bunched.

In the first configuration AGATA 2π can rotate together with PRISMA on a common platform from 20° to 110°. In addition AGATA has two more degrees of freedom, the honeycomb structure can rotate ± 85° around its symmetry axis using the newly commissioned shaft (see Fig. 2). This rotation is needed to install the detectors always horizontally. Another degree of freedom is the distance between the target and the AGATA detectors that can be adjusted from the so-called nominal configuration (distance target to the front of all the various ATC's is equal to 230 mm), to the close-up position, i.e. the whole AGATA array can be translated towards the target by 55 mm. In addition the whole AGATA can be translated backwards up to 750 mm to allow the access to the reaction chamber. In the Zero Degrees configuration (ZD) instead AGATA will be positioned upstream, along the beam line and will be fixed, see Fig. 3, only the rotation around its symmetry axis will be permitted. Compared to the previous GANIL physics campaign, the LNL implementation will allow the installation of up to 27 AGATA Triple Clusters (4 in the inner ring, 9 in the intermediate ring and 14 in the outer ring, see Fig. 4), with a considerable increase of the complexity to deal with all the AGATA services, such as liquid nitrogen distribution, cabling managing, etc. Fifteen flanges (where the detectors are mounted and form the honeycomb, see Fig. 4) were used in the GANIL campaign, while other 15 flanges were newly produced. In order to allow for the rotation of AGATA from 20° to 110° three flanges, number 3, 12 and 26, have been cut to allow the passage of the beam line (see Figs. 2 and 4). A telescopic beam line has been designed to enable the rotations of the whole structure.

Fig. 5 shows the projection, on the target plane perpendicular to the symmetry axis, of the focussing point of each flange accurately, measured using laser tracker. The result of this projection for each flange shows that all the flanges are positioned with a tolerance better than 1 mm, besides two of them, 3 and 26 that as discussed before are cut to allow the passage of the beam line and will not be used to position any detector.

The detector positioning and alignment of the ATC in the structure has been improved with respect to the previous installations in three different aspects. Firstly, the alignment in a mechanical jig that allows to correct the position. This is done with the assistance of the laser

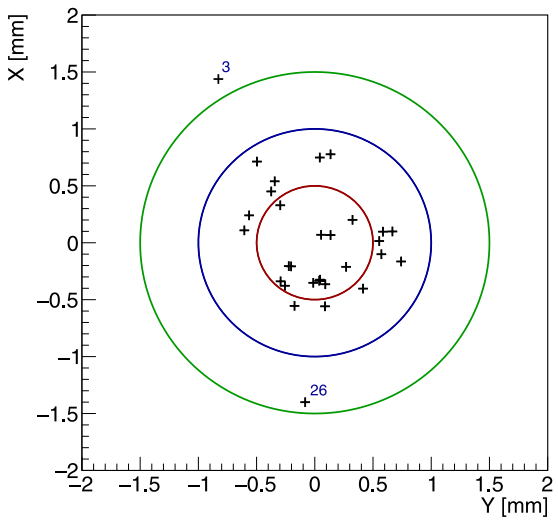

Fig. 5. Projection on the target plane perpendicular to the symmetry axis of the focussing point of each flange, see text for more details.

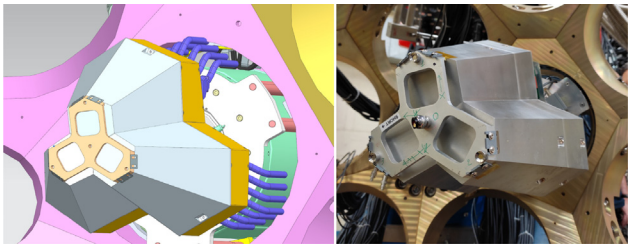

Fig. 6. The new detector alignment tip tool: (a) as designed (b) once in use on the tip of the first inserted detector during the alignment procedure.

tracker. It has been improved by substituting the old aluminium masks with new plastic movable masks, that increases the precision. Using this feature the plastic mask cannot scratch the detector surface and every change in the detector position can be done with the detector fully inserted and fixed into the mechanical Jig. This is the first step to accurately install a detector in the honeycomb structure. When the detector is positioned in the structure, a new add-on to the detector fixing system to the honeycomb has been developed in such a way that using the three holding points of the detectors to the flange, a better control of the detector position during the handling is obtained. Lastly, a new laser tracker alignment tool is available and can be used to ensure the detector tip positioning monitor during all the installation procedure time. The new tool is shown in Fig. 6.

This new procedure with the continuous laser tracker assistance together with the three controlled positioning points allowed for a better detector insertion and extraction from the honeycomb keeping at all times a tip displacement below 0.4 mm.

Fig. 7 shows the (x, y, z) error position of each AGATA Triple Cluster (front of the cryostat end-cap) with respect to the nominal position (230 mm), after the improvement of the detector positioning, obtained with the laser tracker. The average measured distance is 229.95 mm with an average dispersion of 0.11 mm, to be compared with its previous implementation at GANIL, where the average measured distance was 230.9 mm (shown as a rectangle in Fig. 7 with an average dispersion of 0.4 mm).

2.1. Reaction chamber

The design of the scattering chamber for the installation of AGATA coupled to the PRISMA spectrometer had to meet the following criteria:

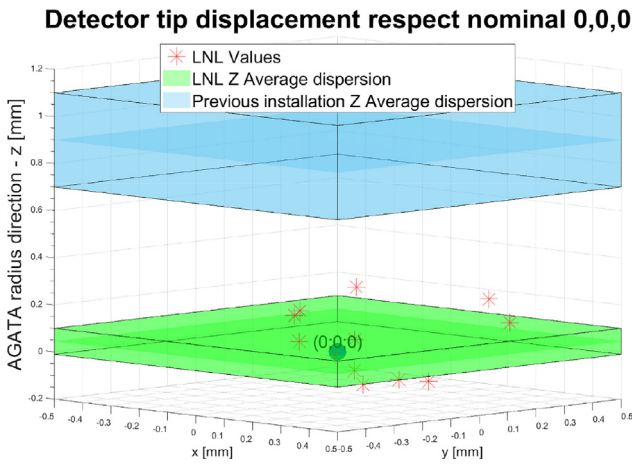

Fig. 7. Coordinates (x, y, z) error position of each AGATA Triple Cluster tip with respect to their nominal position. There is an average dispersion of 0.11 mm, see text for more details. The blue and green rectangle are centered at the average error distance and represent the average dispersion at GANIL and LNL respectively.

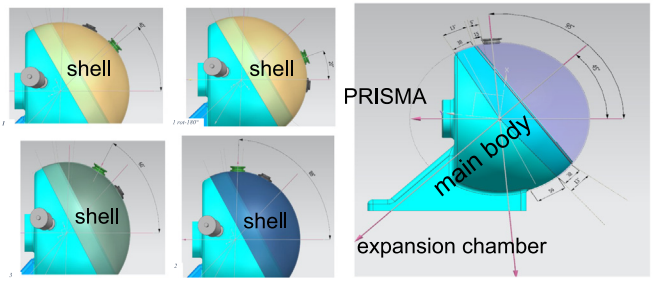

Fig. 8. Right Panel: CAD visualization of the scattering chamber for the installation of AGATA coupled to PRISMA: the light-blue shell (main body of the reaction chamber) is firmly attached to the entrance of the magnetic spectrometer, while the half sphere elements is one of three removable shells (each of the three shells indicated by a different color). The ensemble of the movable shells used to cover the rotation angle between 7–88° are shown in the left panels. Although it is possible to reach mechanically up to 95°, only up to 88° one can perform vacuum. The beam enters via the flange in the removable shell.

(i) reduced thickness to minimize γ-ray absorption; (ii) working range of use between 20° and 85° to allow for a wide set of experiments; (iii) large volume to accommodate complementary detectors; (iv) connection towards a service chamber, also named "expansion chamber", where beam dumps, cables and front-end electronics for the complementary detectors can be placed. Several access and viewports were then envisaged for beam-centering purposes.

The final scattering chamber design comprises two independent shells, one rigidly connected to the entrance of the PRISMA spectrometer, and a set of movable shells that allow us to cover angles ranging from 7°–88°, that warranty the high vacuum. The outer radius of the movable shells is 170 mm, resulting in a large space inside the chamber. The chosen diameter of the chamber allows AGATA to work in the so-called high-efficiency configuration, when the full honeycomb is moved 55 mm towards PRISMA. The chamber consists of the anticorodal Aluminium 6082 alloy with a thickness of 2 mm on the spherical parts, and is reinforced to 5 mm on the flat surface towards PRISMA. The CAD visualization of the scattering chamber is shown in Fig. 8 together with a set of movable shells used to cover the rotation angle between 7–88°.

Finite Elements Analysis (FEA) investigations have been conducted in order to verify possible deformations of the chamber under stress induced by the external pressure when the chamber is at the working vacuum level of 10^{-6} mbar, which confirmed its stability. An additional

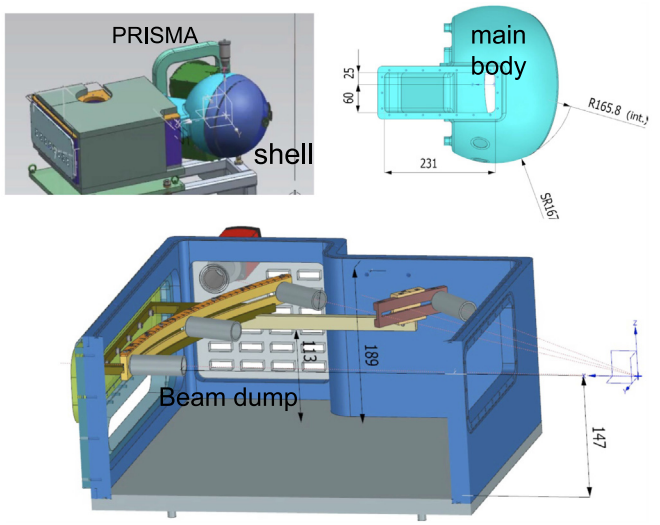

Fig. 9. Details of the expansion chamber. Top left: ensemble of the scattering chamber and the expansion chamber. Top right: side view of the scattering chamber, showing the connecting elements towards the expansion chamber. Bottom panel: inner view of the expansion chamber where the position of the beam dumps and of flanges for connectors is visible. All numbers are in mm.

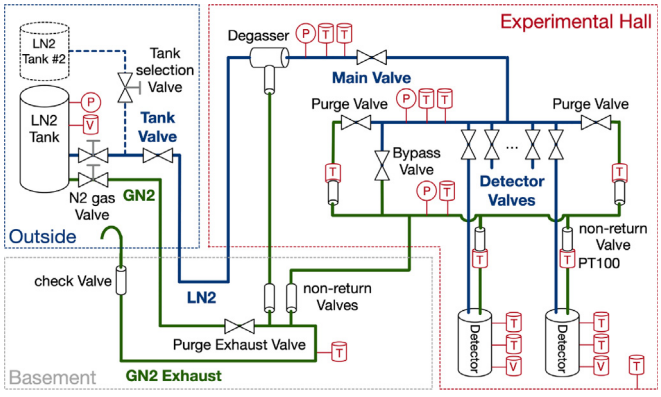

Fig. 10. Scheme of the LN_2 distribution line.

pumping unit is directly attached on the expansion chamber in order to help reaching desired working conditions.

Fig. 9 shows different views of the reaction chamber. The ensemble of the two chambers (reaction and expansion chamber) is shown in the top-left panel. The right panel of Fig. 9 shows a detail of the element connecting the two chambers. The horizontal line marks the beam line height, showing the large space left for the passage of the cables. The bottom panel of Fig. 9 shows the interior of the chamber. A protractor allocates the beam dump at various angles depending on the angular position of PRISMA. Such a protractor is divided in two sections, a forward one, serving angles between 45°–53° (forward beam dump position), and a backward element for larger angles (retracted beam dump position). For angles below 45°, with a minimum value of 20°, the beam dump has to be positioned inside the chamber at 8 cm distance from the target.

The lower part of the expansion chamber is used to host cables and electronics, which are connected to the back and side movables flanges using feed-through connectors. The scattering chamber and the protractors are also made of 6082 Aluminium alloy.

Being the expansion chamber located in close vicinity of the AGATA detector the effect of the presence of the beam dumps has been carefully studied using Geant4 simulations [26]. The study highlighted a strong effect induced by the large connecting section between the two

Table 1
Reference angular ranges and beam dump positions for the AGATA-PRISMA scattering chamber.

AGATA position	PRISMA angle (°)		Beamdump position
	Min.	Max.	
Nominal	20	45	Inside[a]
	45	53	Forward
	53	84.5	Retracted
Close-up	35	45	Inside[a]
	45	53	Forward
	53	88	Retracted

[a]Beamdump inside the reaction chamber, distance to target 8 cm.

chambers, particularly evident when working at angles between 45° and 58°. Thanks to simulations, we decided to shield the expansion chamber with plates of tungsten alloy (25 mm thick) on the side and of lead (40-mm) on the top and bottom, as depicted in top left panel of Fig. 9 in a greenish color.

2.2. Available angular range for grazing reactions

AGATA is expected to work coupled to PRISMA at two distances: the nominal position and the higher-efficiency close-up configuration. However, AGATA can in principle be positioned at any distance from −55 mm (close-up configuration) up to +750 mm. Table 1 shows the final possible angles between of PRISMA with respect to the beam line as well as the beam dump position for each angular range, after considering all the structural limitations for the nominal and the close-up configurations. One should notice that in the nominal position we have an angular range from 20° to 84.5°, while for the close-up position the angular range changes from 35° to 88°. Another general consideration is that for the configurations where the beam dump is inside the reaction chamber a larger background is expected.

2.3. Cryogenic infrastructures

The AGATA HPGe detectors must be maintained at liquid nitrogen (LN_2) temperature during the whole experimental campaign without interruption. A scalable system has been initially considered to avoid major configuration changes of the cryogenic installation in all the laboratories hosting AGATA over time. All attempts to define a common configuration were unsuccessful due to large differences in the existing infrastructures of the host laboratories. Therefore a dedicated design of the LN_2 filling system has been conceived for the AGATA installation at LNL to satisfy both safety constraints, the necessity of a fast response of the system in case of accidental detector warm up and the optimization of the filling procedure and all the mechanical constrains, i.e. allow AGATA to perform the necessary roto-translations. Fig. 10 shows the scheme of the LN_2 distribution line.

The cryogenic liquid is taken from a large volume container (20000 l at 2.3 bar), installed outside the building, and is transported along a super-insulated fixed line inside the experimental room. The whole line (about 45 m long) is kept cold and without residual gases, with the insertion of a degaser before the main control valve. The line terminates with a sequence of two movable arms, connected to a distribution manifold through a metal hose (in vacuum). A metal structure supports the entire line in the experimental room, ensuring the correct movement of the mobile section. To minimize humidity condensation close to the detector electronics, metal hoses (in vacuum) are also used to connect the detectors to the load and exhaust manifolds. The gaseous phase of the degaser, the exit of the safety valves inside the building and the exit of the exhaust manifold are conveyed to the N_2 gaseous evacuation system. The evacuation line is built in steel with vacuum insulation, the outlet is on an external chimney at atmospheric pressure. A N_2

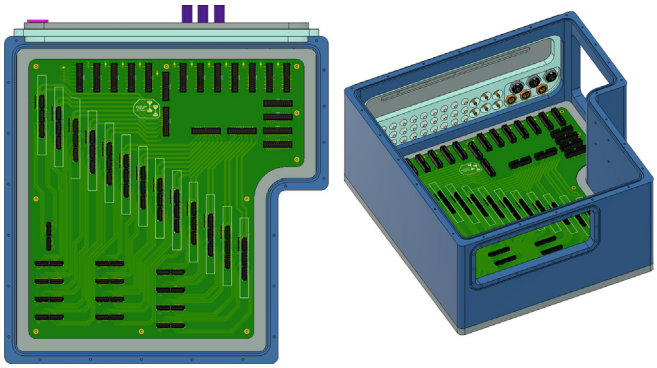

Fig. 11. Top-view and three-quarter-view renderings of the pre-amplifier motherboard. The 64-channel pre-amplifiers are meant to be plugged on the central connectors: the diagonal arranging allows for an easier connection of the flexible kapton PCBs that carry the output signals.

gas socket in the external container ensures efficient emptying of the evacuation line of residual gas.

With the present ATC design (4.5 l Dewar), about 5.2 l of LN_2 are needed for a single detector at every filling cycle. The holding time of the Dewar is relatively short and four fillings per day are necessary. The total LN_2 consumption for an array of 30 ATC is therefore about 160 l per filling cycle, excluding the permanent cooling of the transfer line up to the main valve (≈ 700 l/day). Additional LN_2 (about 20 l) is used at every filling cycle to purge the unwanted N_2 gas and cool the transfer line after the main valve and the manifold. With the LN_2 permanently available close to the detectors (about 7 m), the filling request of a warming up detector can be satisfied in less than 2 min, thus restoring the normal conditions in an acceptable time.

The hardware to monitor and control the LN_2 filling system is based on industrial SIEMENS modules with a scalable architecture (groups of 16 detectors). The installed configuration is for 32 detectors but can be easily extended towards the full 4π array. The correct functioning of the entire distribution system, the filling operations of the detectors and the alarms management are controlled by a PLC using the EPICS software platform and can be accessed via a Graphical User Interface. The EPICS server is also used for data archiving. The system integrates the control of detector and electronics (digitizer) low voltage components and generates the signals to enable/disable the detector HV bias.

Each ATC cryostat is equipped with two Pt100: the primary one is placed along the cold finger, close to the Dewar to monitor the detector behavior and guarantee a fast reaction of the HPGe cooling system; the secondary Pt100 is installed very close to the capsules and in thermal contact with one of them. In addition, the LN_2 level inside the Dewar is determined from a capacitive measurement. Decisions in the filling procedure are based on the Dewar Pt100 with an automatic switch to the second Pt100 (capsule) in case of Pt100 failure. The LN_2 capacity readout is only monitored by the system.

The detector filling sequence is defined/changeable in the "expert" layer of the GUI, according to cryogenic characteristics. Only 4 detectors are filled at once, to limit the maximum number of detector valves open at the same time.

System information and alarm conditions are notified as SMS to the team responsible of monitoring the system via a dialer communicating with the PLC.

3. Data acquisition system

AGATA pre-processing electronics and data acquisition infrastructure (DAQ) at LNL is distributed over two computing centers. The so-called VAX room, 60 m away from the experimental hall has been chosen to host the pre-processing and services related to the early phase electronics. The second place, part of the LNL new computing center, will host the high density servers for the electronics currently under construction to handle all the channels of the 2π array. The distributed acquisition system, DCOD, implemented for AGATA during the last campaign at GANIL [11] is maintained for all the duration of the stay of AGATA at LNL. The complementary detectors presented in this contribution are all readout using digital electronics and the XDAQ distributed DAQ system [27]. The XDAQ applications follow the same logic that has been developed previously at LNL for the GALILEO γ-ray array [28]. The system has been fully upgraded to XDAQ v15 and CentOS-7. On top of this software update, it is worth pointing out that the PRISMA readout chain has been upgraded with respect to the one used during the AGATA-demonstrator phase [3], allowing one to consequently reduce the readout dead-time to less than ∼ 5% at typical rate of 1 kHz and to less than ∼ 15% at 5 kHz.

4. Complementary instrumentation

Complementary detectors are key instruments in γ-ray spectroscopy studies, allowing the investigation of exotic reaction channels, which are characterized by small cross section or large background. The AGATA array can be coupled with a variety of complementary instrumentation to detect light-charged particles, heavy ions, neutrons, high-energy γ rays and measure lifetimes. Moreover, particle detectors can be used to extract additional information on the structure of excited states using particle spectroscopy techniques.

A number of complementary detectors are available when AGATA is at the target position of the magnetic spectrometer PRISMA. In the following the complementary devices will be discussed: EUCLIDES, TRACE, SPIDER, DANTE, $LaBr_3$:Ce, plunger.

4.1. Common motherboard for silicon detector pre-amplifiers

The pre-amplifiers for the silicon detectors are standardized both for the SPIDER and the EUCLIDES arrays (see Sections 4.3 and 4.4). The TRACE array can either use the same electronics or custom integrated pre-amplifiers (see Section 4.5). The detector connections have been standardized and made entirely on flexible kapton PCBs with high-density Samtec connectors. The signals are routed inside the motherboard and connected to the corresponding pre-amplifiers. These are inserted vertically on the motherboard and are placed in a diagonal arrangement in order to make the connection of the output cables easier. The output cables are realized on flexible kapton PCBs and are connected directly on the pre-amp boards and on the flange feed-throughs. All the signals coming from the pre-amplifiers are differential in order to minimize electro-magnetic interference from the large PRISMA magnets. They run on the kapton cables along controlled-impedance 100 Ω differential pairs. The pre-amplifier thermal dissipation is ensured by the connectors to the motherboard, that include a massive central ground contact. The motherboard is thermally coupled to the bottom of the chamber thanks to a thermal gap foil. The motherboard includes also connections for both the various detector high voltages and, if available, for the pre-amplifier digital slow-control. Fig. 11 shows the pre-amplifier motherboard in the expansion chamber.

4.2. Common readout chain

As for the pre-amplifier, the choice was made to build a common readout chain for the complementary devices. The chain is based on commercial digitizers provided by CAEN. So far, both V1725 and V1730 boards were successfully integrated in the readout chain. Those boards are based on 250 MHz and 500 MHz 14-bit ADC chips respectively. To cope with the single-ended signal input, MesyTec MDU-16 16-channels differential-to-unipolar converter are added to the chain. This module offers both the low noise and a large range of analog amplification gain from 1/8 to 12 allowing to cope with the large range of applications foreseen for the Si-detectors array.

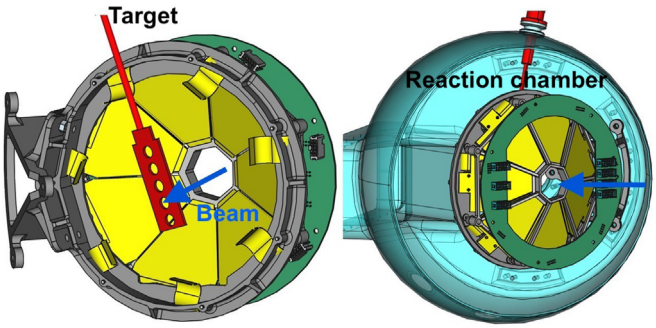

Fig. 12. CAD visualization of SPIDER mounted in the AGATA reaction chamber from the front (left) and back (right) view. SPIDER is shown in yellow, the target holder in red, and the PCB ring in green. In the right figure, the AGATA reaction chamber is also shown, in cyan.

New CAEN V2740 64-channels 125 MHz 16 bit digitizers are currently being implemented in the readout chain to considerably increase the number of available channels. This will be particularly important for TRACE.

4.2.1. Synchronization with AGATA clock system

The CAEN digitizers are not intrinsically compliant with the AGATA Global Trigger and Synchronization (GTS) system. Two points are of particular importance: (i) the AGATA clock distribution is working at 100 MHz; (ii) the clock counter is common to all the AGATA electronic branches and not dependent whether the acquisition is running or not, i.e. it is only reset during the alignment of the GTS tree or once the clock reaches the roll-over over the 48 bit of the 100 MHz counter.

On the CAEN digitizer side the clock counter is reset at each start of the acquisition and its increment depends on the board model and firmware used. The clock signal is internally generated by the boards. Boards can be synchronized between themselves propagating the low-voltage differential signal (LVDS) of the clock from one board to the next or using a LVDS clock-distribution unit. The 100 MHz GTS clock is extracted from a GTS VME carrier, passed through an LVDS fan-in fan-out (DT4700) to be propagated to all necessary boards, thus ensuring the clock synchronization of the two systems. Dedicated Phase-locked loop (PLL) firmware blocks were provided by CAEN for all the different board generation. Clock synchronization is monitored during the data acquisition, constantly checking the PLL-unlock registers of the CAEN digitizers. In case an unlock is detected the run is stopped and restarted.

To obtain a full synchronization of AGATA and the complementary electronics, it is necessary to obtain the value of the GTS clock counter when the CAEN digitizers are started. This part ensures using a common NIM signal propagated to the trigger-in input of the CAEN boards and to the AGAVA VME GTS interface [1]. Both signal generation and readout of the AGAVA buffer is done using a V2718 VME PCI Optical Link Bridge. The control of the board has been directly included into the XDAQ readout application, to be fully transparent for the users.

4.2.2. Participation to the hardware AGATA validation

Depending on the experimental requirement, the complementary instrumentation read by the CAEN digitizer can be included in the validation decision made by the AGATA Trigger Processor (ATP) included in the GTS tree. The trigger-out (TRG-OUT) output of all the boards are OR-ed using a V976 VME coincidence module. The generated OR NIM-signal is then sent to the AGAVA VME board [1] local trigger which generates a GTS trigger request and propagates it to the ATP. By design, once the AGAVA detects a local trigger, the board blocks until the data are read. To avoid large dead-time on the AGAVA board, a VxWorks CPU has been included in the VME crate to flush the buffer of the AGAVA board. Since the AGAVA data are not relevant for the experiment during the data acquisition these data are simply discarded.

4.2.3. Pre-trigger using the AGATA γ-OR

Since the GTS trigger decision is not included in the trigger validation of the complementary instrumentation, due to the latency of the GTS response, a logical signal γ-OR signal can be generated by the AGATA electronics and sent to the complementary instrumentation. Delays of 200–500 ns have been observed depending on the energy of the γ-rays in AGATA. The generation of the γ-OR signal has been simplified with respect to the GANIL implementation, since only early-phase V1 electronics is used. The V1 electronics generate an LVDS trigger signal, based on a settable threshold on the high-gain core signal of the individual crystals. The threshold is set via (i) hardware gross threshold (ii) slow-control fine threshold. Thresholds have been adjusted to include energy as low as possible using the ^{241}Am source 59 keV transition. All LVDS signals are concentrated and sent to a V2495 programmable logic unit. In the present configuration, the V2495 can accept up to 128 LVDS inputs, thus allowing to fully cover all the channels of the 2π AGATA configuration using a single board. Dedicated firmware has been developed for the boards to generate the γ-OR, further improvements are on-going and will make possible for users to set a minimum fold requirement, and better monitor the board response.

4.3. SPIDER

The Silicon PIe DEtectoR (SPIDER) is a modular array of trapezoidal-shaped silicon detectors for charged particles [16], that is used to measure the ions in Coulomb excitation experiments. Each detector is 300 μm thick and segmented into eight independent strips. When used with AGATA, SPIDER consists of 7 detectors arranged in a cone-like shape, as shown in Fig. 12. The detectors are mounted on a 3D-printed aluminium support frame attached to the AGATA reaction chamber at 50° relative to the PRISMA entrance window. The distance between SPIDER and the target position can span from 9 to 11 cm. The angular coverage of SPIDER ranges from 126° to 162° for the 9 cm distance and from 134° to 165° for the 11 cm distance (the angles are given relative to the beam direction). The solid-angle coverage is ≈ 16% and ≈ 12% of the 4π solid angle in the two configurations, respectively.

The energy resolution achievable with SPIDER ranges between 1.5% and 3.3% for 5.5 MeV α particles, increasing with the size of the strip [16]. In Coulomb excitation experiments, the segmentation of the particle detector, together with the position sensitivity of AGATA, allows for achieving energy resolutions after Doppler correction of ≈ 1% or better, for 1 MeV γ-rays. In addition, SPIDER can be coupled with the DANTE micro-channel plate array (see Section 4.6) and with the plunger device (see Section 4.8).

4.4. EUCLIDES

EUCLIDES is an array of 40 $\Delta E - E$ silicon detector telescopes disposed in a 4π configuration and used for the detection of light-charged particles [13], that is used to identify the reaction channels in fusion-evaporation reactions. The array has been successfully used previously as a complementary device for γ-ray arrays in experimental campaigns employing fusion evaporation reactions. The particle identification via the $\Delta E - E$ technique and coincidence measurements with γ rays allows reaching a high reaction channel selectivity event by event. The typical resolution of the silicon detectors of the array range from 1% to 2% at 5.5 MeV.

The full configuration of EUCLIDES can be mounted in the reaction chamber (see Fig. 13) of AGATA surrounding the target and covering 80% of the solid angle. Besides the full configuration, half of the array may be installed in the chamber covering backward angles with respect to the beam direction. This allows the coupling of the array with other complementary detectors.

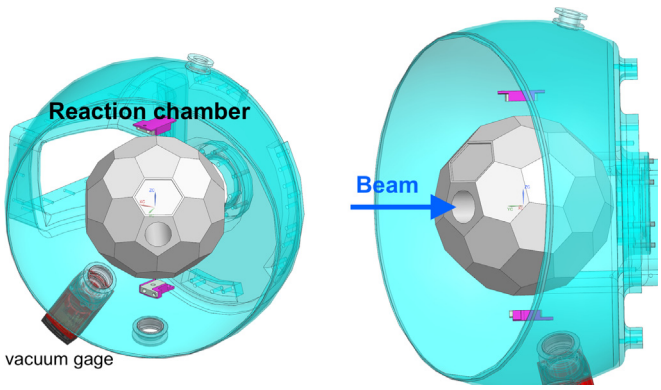

Fig. 13. Two different CAD visualizations of EUCLIDES in gray placed inside the vacuum chamber of AGATA at 44°.

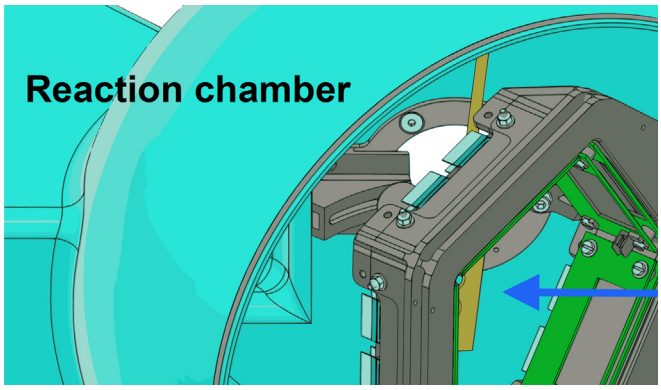

Fig. 14. CAD visualization of the TRACE detector inside the AGATA reaction chamber. The detector PCB supports are in green. The five detectors are mounted on a pentagon-like 3D-printed plastic support that can move by ±10 mm in order to select the desired angular positioning.

4.5. TRACE

TRACE (TRacking Array for light Charged Ejectiles) is an array of segmented silicon detectors in telescope ($\Delta E - E$) configuration aimed at performing spectroscopy and discrimination of charged particles and light ions (see Fig. 14) in transfer reactions. It is made of up to five detectors with an active area of 60 4 × 4 mm^2 square pads arranged in a 12 × 5 configuration. The detectors are arranged in a pentagon-like shape and fixed on a custom 3D-printed frame. The ΔE layer is 200 μm thick while the E layer is 1–1.5 mm thick. Each ΔE pad is acquired independently while the E pads are grouped 15 by 15, although different grouping (or no grouping, with some limitations) are possible. The common back electrode of both crystals is read-out mainly for triggering purpose. In this way each detector outputs a total of 64 anodic channels and 2 cathodic ones. The detectors are placed at a distance of 62 mm from the target and can be moved along the beam axis of ±10 mm. In this way the angular coverage spans from 30°–41° to 40°–57°.

Thanks to the good angular and energy resolution, TRACE can be profitably used to improve the Doppler correction on the HPGe γ spectra. PSA (Pulse-Shape Analysis) is performed on the anodic signals in order to extend the particle-discrimination capabilities [29] of the detectors at low energies [30].

Detectors can be connected either to the common pre-amplifier or to custom-designed low-noise integrated charge-sensitive pre-amplifiers [15,31–33] with a linear dynamic range of 40 MeV extended to up-to 700–800 MeV using the Time-over-threshold technique for saturated signals [34,35].

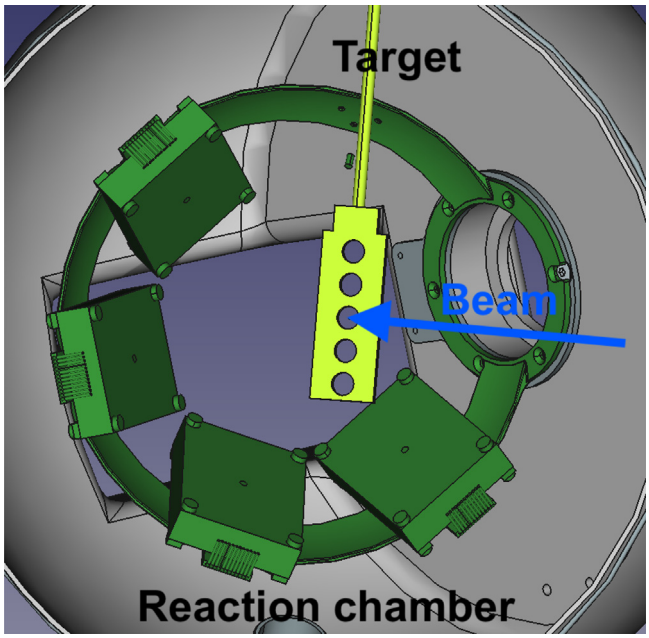

Fig. 15. CAD visualization of four DANTE detectors, in green, mounted in the reaction chamber to cover the forward angles. The target holder in yellow. The AGATA reaction chamber is also shown, in gray.

4.6. DANTE

DANTE (Detector Array for multi-Nucleon Transfer Ejectiles) is an array of Micro-Channel Plate (MCP) detectors designed to detect charged particles and heavy ions [22] in multi-nucleon transfer and fission reactions. The modular array consists of 1–8 single detector units, which can be arranged in different configurations in within the AGATA reaction chamber. The wide range of covered angles, including the forward angles, makes it practical for a broad range of experiments, employing reaction mechanisms such as multi-nucleon transfer [36], fusion–fission and Coulomb excitation. Each detector consists of a Mylar foil which produces the primary electrons when hit by a charged particle, two MCP 40 × 60 mm^2 each, providing a fast-timing signal with a resolution of ∼ 200 ps and two delay-line signals providing the hit position with a resolution of ≤1 mm. Each detector is equipped with a cross mask used for the position calibration. The intrinsic efficiency of a single detector ranges from about ∼70% for light particles, up to ∼100% for heavy ions. The detectors are biased with a 2–3 kV potential. The fast-timing and the signals are pre-amplified with the Philips 6955 amplifiers, processed with Constant Fraction Discriminator (CFD) modules and, for the position determination, then fed to a TAC module. Four DANTE detectors mounted to cover the forward angles within the reaction chamber can be seen in Fig. 15.

DANTE can be coupled to the SPIDER array (see Section 4.3), covering the −20° – +20° angles in ϕ and ∼15° – 75° in θ for the forward-angle configuration or ∼100° – 115° in θ in backward-angle configuration.

4.7. $LaBr_3$:Ce

An array of $LaBr_3$:Ce [37,38] will be coupled to the AGATA array for fast timing measurement and for high-energy γ-ray spectroscopy. The array consist of seven (7) 3”×3” and eight (8) 2”×2” BrilLanCe 380 $LaBr_3$:Ce, produced by Saint Gobain. A total of 10 scintillator detectors will be mounted on the honeycomb as shown in Fig. 16. In order to avoid mechanical clashes with the AGATA triple clusters, the closest possible distance between the front face of the $LaBr_3$:Ce detector and

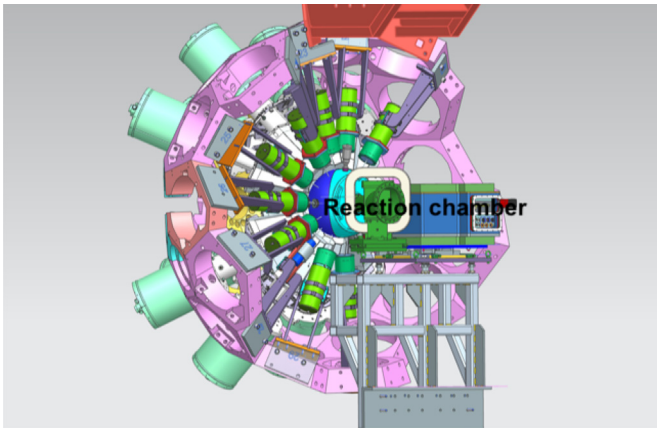

Fig. 16. CAD visualization of the $LaBr_3$:Ce detectors (in green) allocated inside the AGATA honeycomb (in pink).

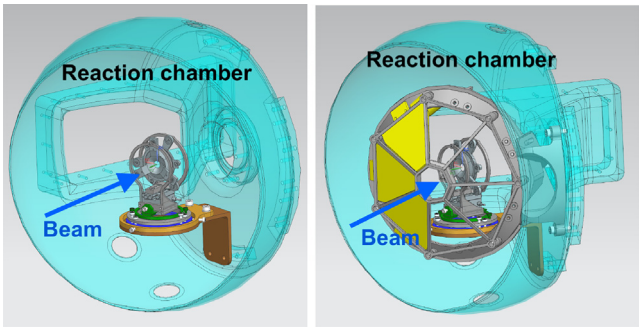

Fig. 17. CAD visualization of the new AGATA plunger. The plunger is placed on the dedicated support that allows the regulation of the position of the device along the three axes and the rotation of it (left). CAD visualization of the plunger coupled to SPIDER (in yellow).

the target position will be of 255 mm. This setup cannot be used in the final 2π configuration where we will have 27 ATCs in the structure.

The measured photo-peak efficiencies using a ^{60}Co source, for the 3" × 3" detectors at 1.3 MeV are around 1.4×10^{-1}% for one scintillator. Simulated photo-peak efficiencies for the smaller size $LaBr_3$:Ce at the closest distance from the target position are expected to lie at around 1.8×10^{-2}%.

4.8. Plunger

The plunger is a device used to measure lifetimes of excited states in the range between 10^{-9} to 10^{-12} s using the Recoil Distance Doppler Shift (RDDS) method [39]. This device allows one to change the distance between the target and a degrader (or stopper) in a range from few micrometers to few millimeters with a sub-micrometric precision.

A new support, presented in Fig. 17, has been designed to be compatible with the reaction chamber of AGATA. The support is connected to the chamber with two screws attached to the side of the chamber close to PRISMA. The height of the support can be regulated with millimetric precision. The support can also move along the XY plane, allowing a horizontal regulation. Finally, the support can rotate in order to adjust the angle of the plunger with respect to the PRISMA spectrometer in experiments at grazing angles. The support material is Aluminium 6082 alloy: this material guarantees a sufficient rigidity that prevents the support from bending under the weight of the plunger.

The new support for the AGATA plunger is compatible to the GALILEO plunger [21] and the Institut für Kernphysik (IKP) three-foil plunger [40] that was designed for AGATA at GANIL. In particular, experiments at 0° using SPIDER can be performed using the GALILEO plunger. On the contrary, experiments involving PRISMA require larger cones of the plunger in order to cover larger angles.

The support has been designed to allow the coupling of the plunger to other complementary devices, in particular to SPIDER, as shown in Fig. 17, and DANTE. In the future, it will be possible to couple the plunger with EUCLIDES.

5. AGATA simulations

Geant4-based simulations are fundamental tools for studying the performances of AGATA and are widely used in data analysis. The AGATA Geant4 code [26,41–43] has been used to optimize the construction of the expansion chamber, by considering different shielding materials in order to minimize the γ-ray background coming from the beam dump (see Section 2.1). The geometry of the chamber has been implemented by importing directly the CAD drawing, using the gdml extension of Geant4. It is important to note that the (x, y, z) coordinate system used in the simulation code is different from the one in the laboratory frame of reference. One can transform one coordinate system into the other by applying a counter-clockwise rotation of 270° with respect to the z axis (which is the same in the two systems).

Two different Geant4 views of 13 ATCs, as installed at LNL, are presented in the panel (a) of Fig. 18. The empty space with missing detectors is used to accommodate the beam pipe. In the pictures, the spherical angular coordinates are shown. In panel (b) of Fig. 18, the simulated efficiency for a 1332-keV γ ray as a function of the AGATA detector angles is displayed in red for the nominal position and in green for the close-up one. The angular efficiency is crucial for planning and analyzing experiments devoted to lifetime measurements.

The simulated detection efficiency for 13 ATCs and for γ rays up to 10 MeV is displayed in Fig. 19. The different sets of points refer to: (i) Calorimeter efficiency, where the energies from all central contacts have been summed up [nominal (red squares) and close-up (green squares)], (ii) Tracking efficiency, i.e. making use of the tracking algorithm [44,45] to reconstruct the traces and energies of the γ rays [nominal (red circles) and close-up (green circles)], and (iii) Core efficiency, where the core energies are directly used without applying the tracking algorithm [nominal (red triangles) and close-up (green triangles)]. For the sake of completeness, we report in Fig. 20 the simulated efficiency for the 2π AGATA configuration including 27 ATCS. Finally, the simulated AGATA efficiency for in-flight γ-ray emission at 1332 keV is shown in Fig. 21 as a function of the nucleus velocity. As observed in the picture, for $\beta = 20\%$ the efficiency decreases from 6% to 4.5%. However, typical $\beta = 10\%$ values or less are expected for the current LNL campaign.

6. Conclusion

The installation of AGATA γ-ray array spectrometer 2π, that will consist of up to 27 ATC has been implemented at Laboratori Nazionali di Legnaro (INFN). The AGATA array is currently coupled to the magnetic spectrometer PRISMA and a second configuration is foreseen with AGATA at Zero Degrees along the beam line. The physics campaign, that started in May 2022, envisages the exploitation of the stable beams from TANDEM-PIAVE-ALPI as well as the radioactive ion beams from SPES to realize an ambitious physics program with AGATA and various complementary detectors such as the PRISMA spectrometer, the particle detectors EUCLIDES, TRACE, SPIDER and GRIT, the neutron detector NEDA, the gamma-ray spectrometer PARIS, the plunger device and the heavy-ion detector DANTE, as well as the cryogenic and gas jet targets CTDIR and SUGAR.

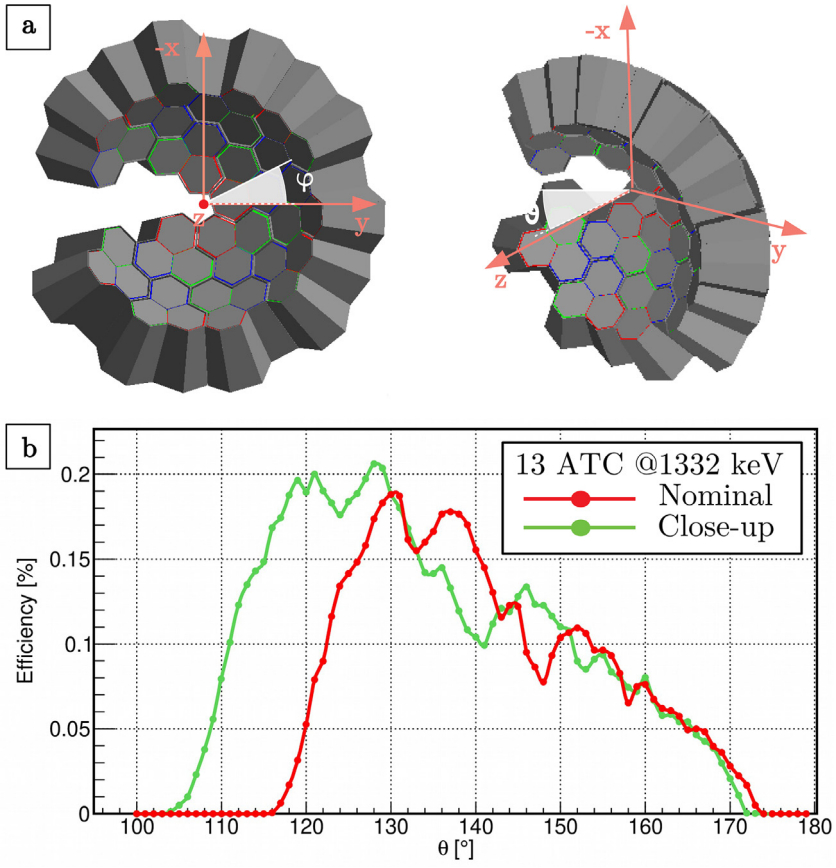

Fig. 18. (a-Left Panel) View of the AGATA array with 13 ATCs, showing the coordinate system. (a-Right Panel) Same as before, rotated view. The θ and ϕ spherical coordinates is indicated in white. (b Panel) Tracking efficiencies for the nominal (red line) and close-up (green line) positions as a function of the θ angle, for a γ ray of 1332 keV. The integrated area under each of the two curves gives the total tracking efficiency at 1332 keV for the associated configuration.

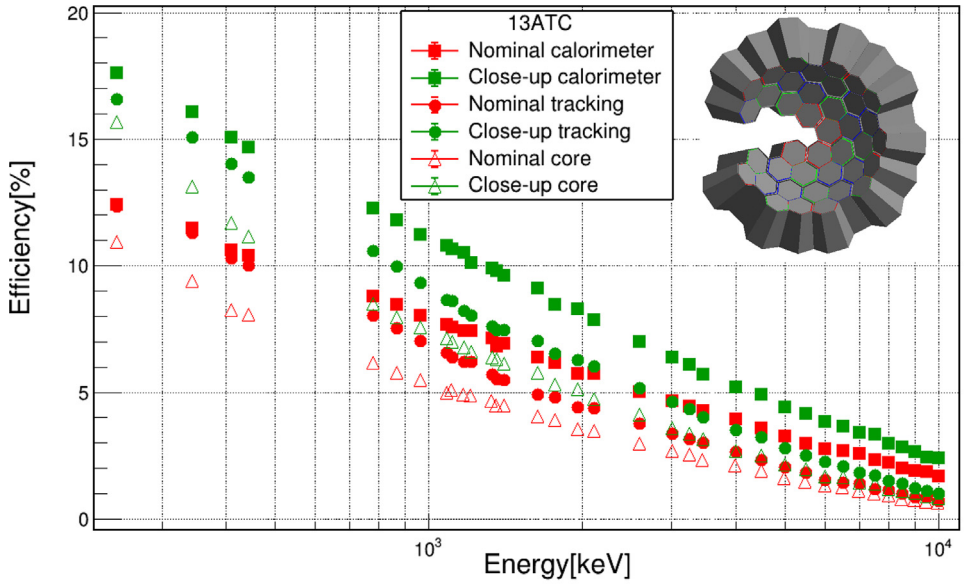

Fig. 19. Calorimeter efficiency [nominal (red squares) and close-up (green squares)], Tracking efficiency [nominal (red circles) and close-up (green circles)], Core efficiency [nominal (red triangles) and close-up (green triangles)]. The simulations consider the AGATA configuration with 13 ATCs. The wide energy range considered goes from 40 keV up to 10 MeV.

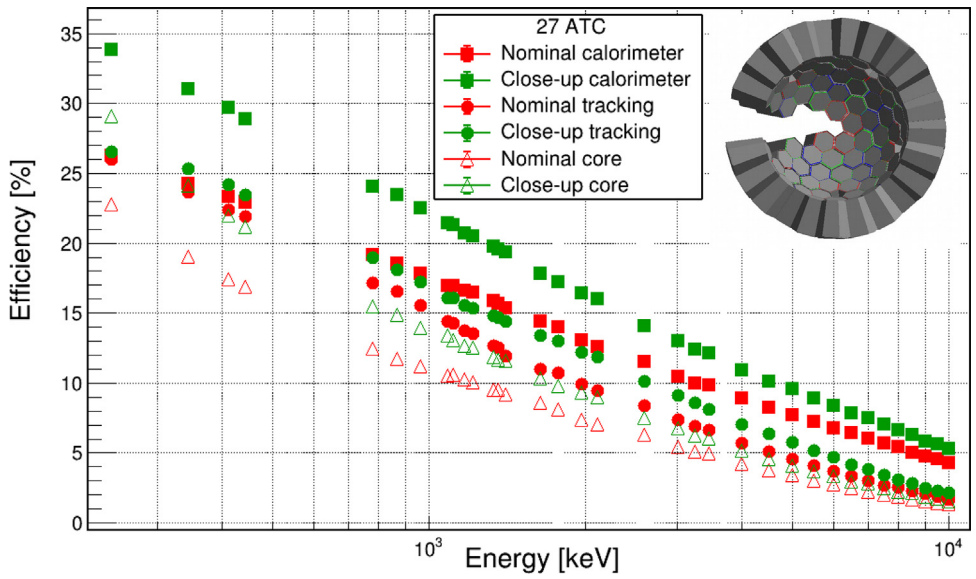

Fig. 20. Calorimeter efficiency [nominal (red squares) and close-up (green squares)], Tracking efficiency [nominal (red circles) and close-up (green circles)], Core efficiency [nominal (red triangles) and close-up (green triangles)]. The simulations consider the AGATA 2π configuration with 27 ATCs.

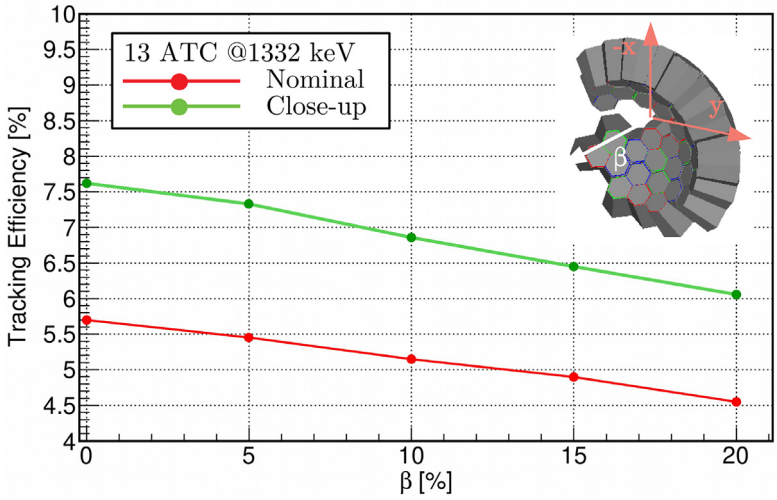

Fig. 21. Tracking efficiency at 1332 keV for the nominal (red) and close-up (green) configurations, as a function of the β=v/c parameter. In the simulation, the AGATA configuration with 13 ATCs was considered and the velocity vector is directed along the z axis.

Declaration of competing interest

The authors declare the following financial interests/personal relationships which may be considered as potential competing interests: Jose Javier Valiente Dobon reports financial support was provided by National Institute of Nuclear Physics Legnaro National Laboratories. Jose Javier Valiente Dobon reports a relationship with National Institute of Nuclear Physics Legnaro National Laboratories that includes: employment.

Data availability

Data will be made available on request.

Acknowledgments

This work was partially supported by MCIN/AEI/ 10.13039/-501100011033, Spain with grant PID2020-118265GB-C42, by Generalitat Valenciana, Spain with grants PROMETEO/2019/005, CIBEST/2021/210 and CIAPOS/2021/114 and by the EU FEDER funds. Partially supported by the Croatian Science Foundation project no. IP-2018-01-1257. Partially supported by the UK Science and Technology Facilities Council including grant ST/T000554/1.

References

[1] S. Akkoyun, A. Algora, B. Alikhani, F. Ameil, G.D. Angelis, L. Arnold, A. Astier, A. Ataç, Y. Aubert, C. Aufranc, A. Austin, S. Aydin, F. Azaiez, S. Badoer, D.L. Balabanski, D. Barrientos, G. Baulieu, R. Baumann, D. Bazzacco, F.A. Beck, T. Beck, P. Bednarczyk, M. Bellato, M.A. Bentley, G. Benzoni, R. Berthier, L. Berti, R. Beunard, G.L. Bianco, B. Birkenbach, P.G. Bizzeti, A.M. Bizzeti-Sona, F.L. Blanc, J.M. Blasco, N. Blasi, D. Bloor, C. Boiano, M. Borsato, D. Bortolato, A. Boston, H.C. Boston, P. Bourgault, P. Boutachkov, A. Bouty, A. Bracco, S. Brambilla, I.P. Brawn, A. Brondi, S. Broussard, B. Bruyneel, D. Bucurescu, I. Burrows, A. Bürger, S. Cabaret, B. Cahan, E. Calore, F. Camera, A. Capsoni, F. Carrio, G. Casati, M. Castoldi, B. Cederwall, J.L. Cercus, V. Chambert, M.E. Chambit, R. Chapman, L. Charles, J. Chavas, E. Clément, P. Cocconi, S. Coelli, P. Coleman-Smith, A. Colombo, S. Colosimo, C. Commeaux, D. Conventi, R.J. Cooper, A. Corsi, A. Cortesi, L. Costa, F.C.L. Crespi, J.R. Cresswell, D.M. Cullen, D. Curien, A. Czermak, D. Delbourg, R. Depalo, T. Descombes, P. Desesquelles, P. Detistov, C. Diarra, F. Didierjean, M.R. Dimmock, Q.T. Doan, C. Domingo-Pardo, M. Doncel, F. Dorangeville, N. Dosme, Y. Drouen, G. Duchene, B. Dulny, J. Eberth, P. Edelbruck, J. Egea, T. Engert, M.N. Erduran, S. Ertürk, C. Fanin,

S. Fantinel, E. Farnea, T. Faul, M. Filliger, F. Filmer, C. Finck, G.D. France, A. Gadea, W. Gast, A. Geraci, J. Gerl, R. Gernhauser, A. Giannatiempo, A. Giaz, L. Gibelin, A. Givechev, N. Goel, V. González, A. Gottardo, X. Grave, J.G. bosz, R. Griffiths, A.N. Grint, P. Gros, L. Guevara, M. Gulmini, A. Görgen, H.T.M. Ha, T. Habermann, L.J. Harkness, H. Harroch, K. Hauschild, C. He, A. Hernández-Prieto, B. Hervieu, H. Hess, T. Hüyük, E. Ince, R. Isocrate, G. Jaworski, A. Johnson, J. Jolie, P. Jones, B. Jonson, P. Joshi, D.S. Judson, A. Jungclaus, M. Kaci, N. Karkour, M. Karolak, A. Kaşkaş, M. Kebbiri, R.S. Kempley, A. Khaplanov, S. Klupp, M. Kogimtzis, I. Kojouharov, A. Korichi, W. Korten, T. Kröll, R. Krücken, N. Kurz, B.Y. Ky, M. Labiche, X. Lafay, L. Lavergne, I.H. Lazarus, S. Leboutelier, F. Lefebvre, E. Legay, L. Legeard, F. Lelli, S.M. Lenzi, S. Leoni, A. Lermitage, D. Lersch, J. Leske, S.C. Letts, S. Lhenoret, R.M. Lieder, D. Linget, J. Ljungvall, A. Lopez-Martens, A. Lotode, S. Lunardi, A. Maj, J.v.d. Marel, Y. Mariette, N. Marginean, R. Marginean, G. Maron, A.R. Mather, W.M. Męczyński, V. Mendez, P. Medina, B. Melon, R. Menegazzo, D. Mengoni, E. Merchan, L. Mihailescu, C. Michelagnoli, J. Mierzejewski, L. Milechina, B. Million, K. Mitev, P. Molini, D. Montanari, S. Moon, F. Morbiducci, R. Moro, P.S. Morrall, O. Möller, A. Nannini, D.R. Napoli, L. Nelson, M. Nespolo, V.L. Ngo, M. Nicoletto, R. Nicolini, Y.L. Noa, P.J. Nolan, M. Norman, J. Nyberg, A. Obertelli, A. Olariu, R. Orlandi, D.C. Oxley, C. Ozben, M. Ozille, C. Oziol, E. Pachoud, M. Palacz, J. Palin, J. Pancin, C. Parisel, P. Pariset, G. Pascovici, R. Peghin, L. Pellegri, A. Perego, S. Perrier, M. Petcu, P. Petkov, C. Petrache, E. Pierre, N. Pietralla, S. Pietri, M. Pignanelli, I. Piqueras, Z. Podolyak, P.L. Pouhalec, J. Pouthas, D. Pugnere, V.F.E. Pucknell, A. Pullia, B. Quintana, R. Raine, G. Rainovski, L. Ramina, G. Rampazzo, G.L. Rana, M. Rebeschini, F. Recchia, N. Redon, M. Reese, P. Reiter, P.H. Regan, S. Riboldi, M. Richer, M. Rigato, S. Rigby, G. Ripamonti, A.P. Robinson, J. Robin, J. Roccaz, J.A. Ropert, B. Rosse, C.R. Alvarez, D. Rosso, B. Rubio, D. Rudolph, F. Saillant, E. Şahin, F. Salomon, M.D. Salsac, J. Salt, G. Salvato, J. Sampson, E. Sanchis, C. Santos, H. Schaffner, M. Schlarb, D.P. Scraggs, D. Seddon, M. Şenyiğit, M.H. Sigward, G. Simpson, J. Simpson, M. Slee, J.F. Smith, P. Sona, B. Sowicki, P. Spolaore, C. Stahl, T. Stanios, E. Stefanova, C. Stahl, J. Strachan, G. Suliman, P.-A. Söderström, J.L. Tain, S. Tanguy, S. Tashenov, C. Theisen, J. Thornhill, F. Tomasi, N. Toniolo, R. Touzery, B. Travers, A. Triossi, M. Tripon, K.M.M. Tun-Lanoe, M. Turcato, C. Unsworth, C.A. Ur, J.J. Valiente-Dobón, V. Vandone, E. Vardaci, R. Venturelli, F. Veronese, C. Veyssiere, E. Viscione, R. Wadsworth, P.M. Walker, N. Warr, C. Weber, D. Weisshaar, D. Wells, O. Wieland, A. Wiens, G. Wittwer, H.J. Wollersheim, F. Zocca, N.V. Zamfir, M. Zięblíński, A. Zucchiatti, AGATA– Advanced gamma tracking array, Nucl. Instrum. Methods Phys. Res. A 668 (2012) 26–58, http://dx.doi.org/10.1016/j.nima.2011.11.081.

[2] S. Paschalis, I. Lee, A. Macchiavelli, C. Campbell, M. Cromaz, S. Gros, J. Pavan, J. Qian, R. Clark, H. Crawford, D. Doering, P. Fallon, C. Lionberger, T. Loew, M. Petri, T. Stezelberger, S. Zimmermann, D. Radford, K. Lagergren, D. Weisshaar, R. Winkler, T. Glasmacher, J. Anderson, C. Beausang, The performance of the Gamma-ray energy tracking in-beam nuclear array GRETINA, Nucl. Instrum. Methods Phys. Res. A 709 (2013) 44–55, http://dx.doi.org/10.1016/j.nima.2013.01.009.

[3] A. Gadea, E. Farnea, J.J. Valiente-Dobon, B. Million, D. Mengoni, et al., Conceptual design and infrastructure for the installation of the first AGATA sub-array at LNL, Nucl. Instrum. Meth. A654 (2011) 88–96, http://dx.doi.org/10.1016/j.nima.2011.06.004.

[4] A.M. Stefanini, L. Corradi, G. Maron, A. Pisent, M. Trotta, A.M. Vinodkumar, S. Beghini, G. Montagnoli, F. Scarlassara, G.F. Segato, A.D. Rosa, G. Inglima, D. Pierroutsakou, M. Romoli, M. Sandoli, G. Pollarolo, A. Latina, The heavy-ion magnetic spectrometer PRISMA, Nuclear Phys. A 701 (1–4) (2002) 217–221, http://dx.doi.org/10.1016/s0375-9474(01)01578-0.

[5] G. Montagnoli, A. Stefanini, M. Trotta, S. Beghini, M. Bettini, F. Scarlassara, V. Schiavon, L. Corradi, B. Behera, E. Fioretto, A. Gadea, A. Latina, S. Szilner, L. Dona, M. Rigato, N. Kondratiev, A.Y. Chizhov, G. Kniajeva, E. Kozulin, I. Pokrovskiy, V. Voskressensky, D. Ackermann, The large-area micro-channel plate entrance detector of the heavy-ion magnetic spectrometer PRISMA, Nucl. Instrum. Methods Phys. Res. A 547 (2–3) (2005) 455–463, http://dx.doi.org/10.1016/j.nima.2005.03.158.

[6] S. Beghini, L. Corradi, E. Fioretto, A. Gadea, A. Latina, G. Montagnoli, F. Scarlassara, A.M. Stefanini, S. Szilner, M. Trotta, A.M. Vinodkumar, The focal plane detector of the magnetic spectrometer PRISMA, Nucl. Instrum. Methods Phys. Res. A 551 (2–3) (2005) 364–374, http://dx.doi.org/10.1016/j.nima.2005.06.058.

[7] S. Szilner, C. Ur, L. Corradi, N. Marginean, G. Pollarolo, A. Stefanini, S. Beghini, B. Behera, E. Fioretto, A. Gadea, B. Guiot, A. Latina, P. Mason, G. Montagnoli, F. Scarlassara, M. Trotta, G. Angelis, F. Vedova, E. Farnea, F. Haas, S. Lenzi, S. Lunardi, R. Marginean, R. Menegazzo, D. Napoli, M. Nespolo, I. Pokrovsky, F. Recchia, M. Romoli, M.D. Salsac, N. Soić, J. Valiente-Dobón, Multinucleon transfer reactions in closed-shell nuclei, Phys. Rev. C 76 (2) (2007) http://dx.doi.org/10.1103/physrevc.76.024604.

[8] N. Pietralla, M. Reese, M. Cortes, F. Ameil, D. Bazzacco, M. Bentley, P. Boutachkov, C. Domingo-Pardo, A. Gadea, J. Gerl, N. Goel, P. Golubev, M. Górska, G. Guastalla, T. Habermann, I. Kojouharov, W. Korten, E. Merchán, S. Pietri, D. Ralet, P. Reiter, D. Rudolph, H. Schaffner, P. Singh, O. Wieland, H. Wollersheim, On the road to FAIR: 1st operation of AGATA in PreSPEC at GSI, EPJ Web Conf. 66 (2014) 02083, http://dx.doi.org/10.1051/epjconf/20146602083.

[9] D. Ralet, S. Pietri, Y. Aubert, M. Bellato, D. Bortolato, S. Brambilla, F. Camera, N. Dosme, A. Gadea, J. Gerl, P. Golubev, X. Grave, H. Johansson, N. Karkour, A. Korichi, N. Kurz, X. Lafay, E. Legay, D. Linget, N. Pietralla, D. Rudolph, H. Schaffner, O. Stezowski, B. Travers, O. Wieland, Collaboration, PreSPEC and AGATA, Data-flow coupling and data-acquisition triggers for the PreSPEC-AGATA campaign at GSI, Nucl. Instrum. Methods Phys. Res. A 786 (2015) 32–39, http://dx.doi.org/10.1016/j.nima.2015.03.025.

[10] N. Lalović, C. Louchart, C. Michelagnoli, R. Perez-Vidal, D. Ralet, J. Gerl, D. Rudolph, T. Arici, D. Bazzacco, E. Clément, A. Gadea, I. Kojouharov, A. Korichi, M. Labiche, J. Ljungvall, A. Lopez-Martens, J. Nyberg, N. Pietralla, S. Pietri, O. Stezowski, Collaborations, For PreSPEC and AGATA, Performance of the AGATA *gamma*-ray spectrometer in the PreSPEC set-up at GSI, Nucl. Instrum. Methods Phys. Res. A 806 (2016) 258–266, http://dx.doi.org/10.1016/j.nima.2015.10.032.

[11] E. Clément, C. Michelagnoli, G. de France, H. Li, A. Lemasson, C. Barthe Dejean, M. Beuzard, P. Bougault, J. Cacitti, J.-L. Foucher, G. Fremont, P. Gangnant, J. Goupil, C. Houarner, M. Jean, A. Lefevre, L. Legeard, F. Legruel, C. Maugeais, L. Ménager, N. Ménard, H. Munoz, M. Ozille, B. Raine, J. Ropert, F. Saillant, C. Spitaels, M. Tripon, P. Vallerand, G. Voltolini, W. Korten, M.-D. Salsac, C. Theisen, M. Zielińska, T. Joannem, M. Karolak, M. Kebbiri, A. Lotode, R. Touzery, C. Walter, A. Korichi, J. Ljungvall, A. Lopez-Martens, D. Ralet, N. Dosme, X. Grave, N. Karkour, X. Lafay, E. Legay, I. Kojouharov, C. Domingo-Pardo, A. Gadea, R. Pérez-Vidal, J. Civera, B. Birkenbach, J. Eberth, H. Hess, L. Lewandowski, P. Reiter, A. Nannini, G. De Angelis, G. Jaworski, P. John, D. Napoli, J. Valiente-Dobón, D. Barrientos, D. Bortolato, G. Benzoni, A. Bracco, S. Brambilla, F. Camera, F. Crespi, S. Leoni, B. Million, A. Pullia, O. Wieland, D. Bazzacco, S. Lenzi, S. Lunardi, R. Menegazzo, D. Mengoni, F. Recchia, M. Bellato, R. Isocrate, F. Egea Canet, F. Didierjean, G. Duchêne, R. Baumann, M. Brucker, E. Dangelser, M. Filliger, H. Friedmann, G. Gaudiot, J.-N. Grapton, H. Kocher, C. Mathieu, M.-H. Sigward, D. Thomas, S. Veeramootoo, J. Dudouet, O. Stézowski, C. Aufranc, Y. Aubert, M. Labiche, J. Simpson, I. Burrows, P. Coleman-Smith, A. Grant, I. Lazarus, P. Morrall, V. Pucknell, A. Boston, D. Judson, N. Lalović, J. Nyberg, J. Collado, V. González, I. Kuti, B. Nyakó, A. Maj, M. Rudigier, Conceptual design of the AGATA 1π array at GANIL, Nucl. Instrum. Methods Phys. Res. A 855 (2017) 1–12, http://dx.doi.org/10.1016/j.nima.2017.02.063, URL https://www.sciencedirect.com/science/article/pii/S0168900217302590.

[12] T. Marchi, G. Prete, F. Gramegna, A. Andrighetto, P. Antonini, M. Ballan, M. Bellato, L. Bellan, D. Benini, G. Bisoffi, J. Bermudez, G. Benzoni, D. Bortolato, F. Borgna, A. Calore, S. Canella, S. Carturan, N. Ciatara, M. Cinausero, P. Cocconi, A. Cogo, D. Conventi, V. Conte, M. Comunian, L. Costa, S. Corradetti, G.D. Angelis, C.D. Martinis, P.D. Ruvo, J. Esposito, E. Fagotti, D. Fabris, P. Favaron, E. Fioretto, A. Galata, F. Gelain, M. Giacchini, D. Giora, A. Gottardo, M. Gulmini, M. Lollo, A. Lombardi, M. Manzolaro, M. Maggiore, D. Maniero, P.F. Mastinu, A. Monetti, F. Pasquato, R. Pegoraro, A. Pisent, M. Poggi, S. Pavinato, L. Pranovi, D. Pedretti, C. Roncolato, M. Rossignoli, L. Sarchiapone, D. Scarpa, J.J. Valiente Dob'on, V. Volpe, A. Vescovo, D. Zafiropoulos, The SPES facility at Legnaro National Laboratories, J. Phys. Conf. Ser. 1643 (1) (2020) 012036, http://dx.doi.org/10.1088/1742-6596/1643/1/012036.

[13] D. Testov, D. Mengoni, A. Goasduff, A. Gadea, R. Isocrate, P.R. John, G. de Angelis, D. Bazzacco, C. Boiano, A. Boso, P. Cocconi, J.A. Dueñas, F.J. Egea Canet, L. Grassi, K. Hadyńska-Klęk, G. Jaworski, S. Lunardi, R. Menegazzo, D.R. Napoli, F. Recchia, M. Siciliano, J.J. Valiente-Dobón, The 4π highly-efficient light-charged-particle detector EUCLIDES,f installed at the GALILEO array for in-beam γ-ray spectroscopy, Eur. Phys. J. A 55 (4) (2019) 47, http://dx.doi.org/10.1140/epja/i2019-12714-6.

[14] J. Bradbury, D. Testov, S. Bakes, A. Goasduff, D. Mengoni, J. Valiente-Dobón, G. de Angelis, D. Bazzacco, C. Boiano, A. Boso, B. Cederwall, M. Cicerchia, G. Colucci, P. Čolović, F. Didierjean, M. Doncel, J. Dueñas, F. Galtarossa, A. Gozzelino, K. Hadyńska-Klęk, G. Jaworski, P. John, H. Liu, S. Lenzi, S. Lunardi, R. Menegazzo, A. Mentana, C. Müller-Gatermann, D. Napoli, G. Pasqualato, F. Recchia, M. Rocchini, S. Riccetto, B. Saygi, M. Siciliano, Y. Sobolev, S. Szilner, Lifetime measurements using a plunger device and the EUCLIDES Si array at the GALILEO γ-ray spectrometer, Nucl. Instrum. Methods Phys. Res. A 979 (2020) 164345, http://dx.doi.org/10.1016/j.nima.2020.164345, URL https://www.sciencedirect.com/science/article/pii/S0168900220307427.

[15] S. Capra, et al., Performance of the new integrated front-end electronics of the TRACE array commissioned with an early silicon detector prototype, Nucl. Instrum. Methods Phys. Res. A 935 (2019) 178–184, http://dx.doi.org/10.1016/j.nima.2019.05.039.

[16] M. Rocchini, K. Hadyńska-Klęk, A. Nannini, J. Valiente-Dobón, A. Goasduff, D. Testov, D. Mengoni, P. John, M. Siciliano, B. Melon, P. Sona, M. Ottanelli, A. Perego, M. Chiari, M. Zielińska, D. Bazzacco, G. Benzoni, S. Bettarini, M. Brianzi, F. Camera, P. Cocconi, C. Czelusniak, D. Doherty, M. Komorowska, N. Marchini, M. Matejska-Minda, P. Napiorkowski, E. Pasquali, L. Ramina, M. Rampazzo, F. Recchia, D. Rosso, L. Sottili, A. Tredici, SPIDER: A silicon PIe detector for low-energy Coulomb-excitation measurements, Nucl. Instrum. Methods Phys. Res. A 971 (2020) 164030, http://dx.doi.org/10.1016/j.nima.2020.164030, URL https://www.sciencedirect.com/science/article/pii/S0168900220304691.

[17] R. Aliaga, V. Herrero-Bosch, S. Capra, A. Pullia, J. Dueñas, L. Grassi, A. Triossi, C. Domingo-Pardo, R. Gadea, V. González, T. Hüyük, E. Sanchís, A. Gadea, D. Mengoni, Conceptual design of the TRACE detector readout using a compact, dead time-less analog memory ASIC, Nucl. Inst. Meth. Phys. Res. A 800 (2015) 34–39, http://dx.doi.org/10.1016/j.nima.2015.07.067, URL https://www.sciencedirect.com/science/article/pii/S0168900215009286.

[18] GRIT web page. URL http://grit.in2p3.fr/.

[19] J.J. Valiente-Dobon, G. Jaworski, A. Goasduff, F.J. Egea, V. Modamio, T. Hüyük, A. Triossi, M. Jastrzab, P.-A. Söderström, A.D. Nitto, G.D. Angelis, G.D. France, N. Erduran, A. Gadea, M. Moszyński, J. Nyberg, M. Palacz, R. Wadsworth, R. Aliaga, C. Aufranc, M. Bézard, G. Baulieu, E. Bissiato, A. Boujrad, I. Burrows, S. Carturan, P. Cocconi, G. Colucci, D. Conventi, M. Cordwell, S. Coudert, J.M. Deltoro, L. Ducroux, T. Dupasquier, S. Erturk, X. Fabian, V. González, A. Grant, K. Hadynska-Klek, A. Illana, M.L. Jurado-Gomez, M. Kogimtzis, I. Lazarus, L. Legeard, J. Ljungvall, G. Pasqualato, R.M. Pérez-Vidal, A. Raggio, D. Ralet, N. Redon, F. Saillant, B. Sayğı, E. Sanchis, M. Scarcioffolo, M. Siciliano, D. Testov, C. Stahl, M. Tripon, I. Zanon, NEDA—NEutron detector array, Nucl. Instrum. Methods Phys. Res. A 927 (2019) 81–86, http://dx.doi.org/10.1016/j.nima.2019.02.021.

[20] A. Maj, The Paris project, Acta Phys. Polon. B 40 (2009) 565.

[21] C. Müller-Gatermann, F. von Spee, A. Goasduff, D. Bazzacco, M. Beckers, T. Braunroth, A. Boso, P. Cocconi, G. de Angelis, A. Dewald, C. Fransen, A. Goldkuhle, A. Gottardo, A. Gozzelino, K. Hadyńska-Klęk, G. Jawroski, P. John, J. Jolie, S. Lenzi, J. Litzinger, R. Menegazzo, D. Mengoni, D. Napoli, F. Recchia, M. Siciliano, D. Testov, S. Thiel, J. Valiente-Dobón, K. Zell, A new dedicated plunger device for the GALILEO γ-ray detector array, Nucl. Instrum. Methods Phys. Res. A 920 (2019) 95–99, http://dx.doi.org/10.1016/j.nima.2018.12.077, URL https://www.sciencedirect.com/science/article/pii/S0168900218318916.

[22] A. Gottardo, J. Valiente-Dobon, Performance of the DANTE detector, Nuclear Phys. A 805 (2008) 606, http://dx.doi.org/10.1016/j.nuclphysa.2008.02.206.

[23] M. Sedlak, A. Gottardo, A. Goasduff, R. Pengo, F. Crespi, I. Lombardo, I. Zanon, The cryogenic targets for direct reactions (CTADIR) project, Nuovo Cim. C 45 (2022) 1–4, http://dx.doi.org/10.1393/ncc/i2022-22108-6, URL https://www.sif.it/riviste/sif/ncc/econtents/2022/045/05/article/16.

[24] F. Favela, L. Acosta, E. Andrade, V. Araujo, A. Huerta, O.G. de Lucio, G. Murillo, M.E. Ortiz, R. Policroniades, P. Santa Rita, A. Varela, E. Chávez, New supersonic gas jet target for low energy nuclear reaction studies, Phys. Rev. Accel. Beams 18 (2015) 123502, http://dx.doi.org/10.1103/PhysRevSTAB.18.123502, URL https://link.aps.org/doi/10.1103/PhysRevSTAB.18.123502.

[25] A. Bracco, G. Duchene, Z. Podolyak, P. Reiter, Gamma spectroscopy with AGATA in its first phases: New insights in nuclear excitations along the nuclear chart, Prog. Part. Nucl. Phys. 121 (2021) 103887, http://dx.doi.org/10.1016/j.ppnp.2021.103887.

[26] AGATA Geant4 simulation code. URL http://npg.dl.ac.uk/svn/agata.

[27] J. Gutleber, S. Murray, L. Orsini, Towards a homogeneous architecture for high-energy physics data acquisition systems, Comput. Phys. Comm. 153 (2) (2003) 155, http://dx.doi.org/10.1016/S0010-4655(03)00161-9.

[28] A. Goasduff, D. Mengoni, F. Recchia, J. Valiente-Dobón, R. Menegazzo, G. Benzoni, D. Barrientos, M. Bellato, N. Bez, M. Biasotto, N. Blasi, C. Boiano, A. Boso, S. Bottoni, A. Bracco, S. Brambilla, D. Brugnara, F. Camera, S. Capra, A. Capsoni, P. Cocconi, S. Coelli, M. Cortés, F. Crespi, G. de Angelis, F. Egea, C. Fanin, S. Fantinel, A. Gadea, E. Gamba, A. Gambalonga, C. Gesmundo, G. Gosta, A. Gottardo, A. Gozzelino, E. Gregor, M. Gulmini, J. Ha, K. Hadyńska-Klek, A. Illana, R. Isocrate, G. Jaworski, P. John, S. Lenzi, S. Leoni, S. Lunardi, M. Magalini, N. Marchini, B. Million, V. Modamio, A. Nannini, D. Napoli, G. Pasqualato, J. Pellumaj, R. Pérez-Vidal, S. Pigliapoco, M. Polettini, C. Porzio, A. Pullia, L. Ramina, G. Rampazzo, M. Rampazzo, M. Rebeschini, K. Rezynkina, M. Rocchini, M. Romanato, D. Rosso, A. Saltarelli, M. Scarcioffolo, M. Siciliano, D. Testov, D. Tomasella, F. Tomasi, N. Toniolo, C. Ur, S. Ventura, F. Veronese, E. Viscione, V. Volpe, O. Wieland, I. Zanon, S. Ziliani, G. Zhang, D. Bazzacco, The GALILEO γ-ray array at the Legnaro National Laboratories, Nucl. Inst. Meth. Phys. Res. A 1015 (2021) 165753, http://dx.doi.org/10.1016/j.nima.2021.165753, URL https://www.sciencedirect.com/science/article/pii/S0168900221007385.

[29] A. Badalà, et al., Trends in particle and nuclei identification techniques in nuclear physics experiments, Riv. Del Nuovo Cimento 45 (3) (2022) 189–277, http://dx.doi.org/10.1007/s40766-021-00028-5.

[30] N. Cieplicka-Oryńczak, et al., Towards the lowest-energy limit for light ions identification with silicon pixel-type detectors, Eur. Phys. J. A 54 (12) (2018) http://dx.doi.org/10.1140/epja/i2018-12644-9.

[31] S. Capra, A. Pullia, Design and experimental validation of an integrated multi-channel charge amplifier for solid-state detectors with innovative spectroscopic range booster, IEEE Trans. Nucl. Sci. 67 (8) (2020) 1877–1884, http://dx.doi.org/10.1109/TNS.2020.3006892.

[32] E. Suerra, et al., A new method for spatial mode shifting of stabilized optical cavities for the generation of dual-color X-rays, Nucl. Instrum. Methods Phys. Res., A 1019 (2021) http://dx.doi.org/10.1016/j.nima.2021.165852.

[33] S. Capra, Impedance and noise closed-form model of large-area integrated resistors with high stray capacitance to be used as feedback discharge devices in charge-sensitive preamplifiers for nuclear spectroscopy, IEEE Trans. Nucl. Sci. 67 (4) (2020) 722–731, http://dx.doi.org/10.1109/TNS.2020.2975311.

[34] A. Pullia, S. Capra, Experimental performance of a highly-innovative low-noise charge-sensitive preamplifier with integrated range-booster, J. Instrum. 13 (12) (2018) http://dx.doi.org/10.1088/1748-0221/13/12/C12004.

[35] S. Capra, G. Secci, A. Pullia, An innovative analog circuit to retrieve energy information from signals of deeply saturated preamplifiers connected to semiconductor detectors, IEEE Trans. Nucl. Sci. 69 (7) (2022) 1757–1764, http://dx.doi.org/10.1109/TNS.2022.3178760.

[36] A. Vogt, B. Birkenbach, P. Reiter, L. Corradi, T. Mijatović, D. Montanari, S. Szilner, D. Bazzacco, M. Bowry, A. Bracco, B. Bruyneel, F.C.L. Crespi, G.D. Angelis, P. Desesquelles, J. Eberth, E. Farnea, E. Fioretto, A. Gadea, K. Geibel, A. Gengelbach, A. Giaz, A. Gorgen, A. Gottardo, J. Grebosz, H. Hess, P.R. John, J. Jolie, D.S. Judson, A. Jungclaus, W. Korten, S. Leoni, S. Lunardi, R. Menegazzo, D. Mengoni, C. Michelagnoli, G. Montagnoli, D. Napoli, L. Pellegri, G. Pollarolo, A. Pullia, B. Quintana, F. Radeck, F. Recchia, D. Rosso, E. Sahin, M.D. Salsac, F. Scarlassara, P.-A. Soderstrom, A.M. Stefanini, T. Steinbach, C. Stahl, B. Szpak, C. Theisen, C. Ur, J.J. Valiente-Dobón, V. Vandone, A. Wiens, Light and heavy transfer products in Xe136+U238 multinucleon transfer reactions, Phys. Rev. C 92 (2) (2015) 12–024619, http://dx.doi.org/10.1103/physrevc.92.024619.

[37] W. Higgins, A. Churilov, E. Van Loef, J. Glodo, M. Squillante, K. Shah, Crystal growth of large diameter LaBr3: Ce and CeBr3, J. Cryst. Growth 310 (7–9) (2008) 2085–2089.

[38] A. Giaz, L. Pellegri, S. Riboldi, F. Camera, N. Blasi, C. Boiano, A. Bracco, S. Brambilla, S. Ceruti, S. Coelli, et al., Characterization of large volume 3.5 × 8 $LaBr_3$: Ce detectors, Nucl. Instrum. Methods Phys. Res. A 729 (2013) 910–921.

[39] A. Dewald, O. Möller, P. Petkov, Developing the recoil distance Doppler-shift technique towards a versatile tool for lifetime measurements of excited nuclear states, Prog. Part. Nucl. Phys. 67 (3) (2012) 786–839, http://dx.doi.org/10.1016/j.ppnp.2012.03.003, URL https://www.sciencedirect.com/science/article/pii/S0146641012000713.

[40] M. Beckers, A. Dewald, C. Fransen, K. Arnswald, C. Muller-Gatermann, F.v. Spee, Development of the multi-purpose cologne compact differential plunger (CoCoDiff) for the measurement of nuclear level lifetimes with the recoil distance Doppler-shift method, Nucl. Instrum. Methods Phys. Res. A 1042 (2022) 167418, http://dx.doi.org/10.1016/j.nima.2022.167418.

[41] S. Agostinelli, J. Allison, K. Amako, J. Apostolakis, H. Araujo, P. Arce, M. Asai, D. Axen, S. Banerjee, G. Barrand, F. Behner, L. Bellagamba, J. Boudreau, L. Broglia, A. Brunengo, H. Burkhardt, S. Chauvie, J. Chuma, R. Chytracek, G. Cooperman, G. Cosmo, P. Degtyarenko, A. Dell'Acqua, G. Depaola, D. Dietrich, R. Enami, A. Feliciello, C. Ferguson, H. Fesefeldt, G. Folger, F. Foppiano, A. Forti, S. Garelli, S. Giani, R. Giannitrapani, D. Gibin, J.G. Cadenas, I. Gonzalez, G.G. Abril, G. Greeniaus, W. Greiner, V. Grichine, A. Grossheim, S. Guatelli, P. Gumplinger, R. Hamatsu, K. Hashimoto, H. Hasui, A. Heikkinen, A. Howard, V. Ivanchenko, A. Johnson, F. Jones, J. Kallenbach, N. Kanaya, M. Kawabata, Y. Kawabata, M. Kawaguti, S. Kelner, P. Kent, A. Kimura, T. Kodama, R. Kokoulin, M. Kossov, H. Kurashige, E. Lamanna, T. Lampon, V. Lara, V. Lefebure, F. Lei, M. Liendl, W. Lockman, F. Longo, S. Magni, M. Maire, E. Medernach, K. Minamimoto, P.M.d. Freitas, Y. Morita, K. Murakami, M. Nagamatu, R. Nartallo, P. Nieminen, T. Nishimura, K. Ohtsubo, M. Okamura, S. O'Neale, Y. Oohata, K. Paech, J. Perl, A. Pfeiffer, M. Pia, F. Ranjard, A. Rybin, S. Sadilov, E.D. Salvo, G. Santin, T. Sasaki, N. Savvas, Y. Sawada, S. Scherer, S. Sei, V. Sirotenko, D. Smith, N. Starkov, H. Stoecker, J. Sulkimo, M. Takahata, S. Tanaka, E. Tcherniaev, E.S. Tehrani, M. Tropeano, P. Truscott, H. Uno, L. Urban, P. Urban, M. Verderi, A. Walkden, W. Wander, H. Weber, J. Wellisch, T. Wenaus, D. Williams, D. Wright, T. Yamada, H. Yoshida, D. Zschiesche, Collaboration, Geant4, Geant4, a simulation toolkit, Nucl. Instrum. Methods Phys. Res. A 506 (3) (2003) 250–303, http://dx.doi.org/10.1016/s0168-9002(03)01368-8.

[42] J. Allison, K. Amako, J. Apostolakis, H. Araujo, P.A. Dubois, M. Asai, G. Barrand, R. Capra, S. Chauvie, R. Chytracek, G.A.P. Cirrone, G. Cooperman, G. Cosmo, G. Cuttone, G.G. Daquino, M. Donszelmann, M. Dressel, G. Folger, F. Foppiano, J. Generowicz, V. Grichine, S. Guatelli, P. Gumplinger, A. Heikkinen, I. Hrivnacova, A. Howard, S. Incerti, V. Ivanchenko, T. Johnson, F. Jones, T. Koi, R. Kokoulin, M. Kossov, H. Kurashige, V. Lara, S. Larsson, F. Lei, O. Link, F. Longo, M. Maire, A. Mantero, B. Mascialino, I. McLaren, P.M. Lorenzo, K. Minamimoto, K. Murakami, P. Nieminen, L. Pandola, S. Parlati, L. Peralta, J. Perl, A. Pfeiffer, M.G. Pia, A. Ribon, P. Rodrigues, G. Russo, S. Sadilov, G. Santin, T. Sasaki, D. Smith, N. Starkov, S. Tanaka, E. Tcherniaev, B. Tom, A. Trindade, P. Truscott, L. Urban, M. Verderi, A. Walkden, J.P. Wellisch, D.C. Williams, D. Wright, H. Yoshida, Geant4 developments and applications, IEEE Trans. Nucl. Sci. 53 (1) (2006) 270–278, http://dx.doi.org/10.1109/tns.2006.869826.

[43] J. Allison, K. Amako, J. Apostolakis, P. Arce, M. Asai, T. Aso, E. Bagli, A. Bagulya, S. Banerjee, G. Barrand, B. Beck, A. Bogdanov, D. Brandt, J. Brown, H. Burkhardt, P. Canal, D. Cano-Ott, S. Chauvie, K. Cho, G. Cirrone, G. Cooperman, M. Cortes-Giraldo, G. Cosmo, G. Cuttone, G. Depaola, L. Desorgher, X. Dong, A. Dotti, V. Elvira, G. Folger, Z. Francis, A. Galoyan, L. Garnier, M. Gayer, K. Genser, V. Grichine, S. Guatelli, P. Guye, P. Gumplinger, I. Howard, S. Hwang, S. Incerti, A. Ivanchenko, V. Ivanchenko, F. Jones, S. Jun, P. Kaitaniemi, N. Karakatsanis, M. Karamitrosi, M. Kelsey, A. Kimura, T. Koi, H. Kurashige, A. Lechner, S. Lee, F. Longo, M. Maire, D. Mancusi, A. Mantero, E. Mendoza, B. Morgan, K. Murakami, T. Nikitina, L. Pandola, P. Paprocki, J. Perl, I. Petrović, M. Pia, W. Pokorski, J.

Quesada, M. Raine, M. Reis, A. Ribon, A.R. Fira, F. Romano, G. Russo, G. Santin, T. Sasaki, D. Sawkey, J. Shin, I. Strakovsky, A. Taborda, S. Tanaka, B. Tom, T. Toshito, H. Tran, P. Truscott, L. Urban, V. Uzhinsky, J. Verbeke, M. Verderi, B. Wendt, H. Wenzel, D. Wright, D. Wright, T. Yamashita, J. Yarba, H. Yoshida, Recent developments in Geant4, Nucl. Instrum. Methods Phys. Res. A 835 (2016) 186–225, http://dx.doi.org/10.1016/j.nima.2016.06.125.

[44] A. Lopez-Martens, K. Hauschild, A. Korichi, J. Roccaz, J.P. Thibaud, Gamma-ray tracking algorithms: A comparison, Nucl. Instrum. Methods Phys. Res. A 533 (2004) 454–466, http://dx.doi.org/10.1016/j.nima.2004.06.154.

[45] Bazzacco, On behalf of the AGATA, The advanced Gamma ray tracking array AGATA, Nuclear Phys. A 746 (2004) 248–254, http://dx.doi.org/10.1016/j.nuclphysa.2004.09.148.16.